DOE/NASA/0161-6
NASA CR-165190

CELL MODULE AND FUEL CONDITIONER

5TH QUARTERLY REPORT: OCTOBER-DECEMBER, 1980

D.Q. Hoover, Jr.
Westinghouse R&D Center
Westinghouse Electric Corporation
Pittsburgh, PA. 15235

January, 1981

Prepared for
NATIONAL AERONAUTICS AND SPACE ADMINISTRATION
Lewis Research Center
Under Contract DEN 3-161

for
U.S. DEPARTMENT OF ENERGY
Energy Technology
Division of Fossil Fuel Utilization
Under Interagency Agreement DE-AI-01-80ET17088

D17-59

DOE/NASA/0161-6
NASA CR-165190

CELL MODULE & FUEL CONDITIONER DEVELOPMENT

5TH QUARTERLY REPORT: OCTOBER-DECEMBER, 1980

D.Q. Hoover, Jr.
Westinghouse R&D Center
Westinghouse Electric Corporation

January, 1981

Prepared for
NATIONAL AERONAUTICS AND SPACE ADMINISTRATION
Lewis Research Center
Under Contract DEN 3-161

for
U.S. DEPARTMENT OF ENERGY
Energy Technology
Division of Fossil Fuel Utilization

TABLE OF CONTENTS

I. INTRODUCTION

This report is for the second Phase of a six Phase program to develop commercially viable on-site integrated energy systems (OS/IES) using phosphoric acid fuel cell (PAFC) modules to convert fuel to electricity. Phase II is a planned two year effort to develop appropriate fuel cell module and fuel conditioner conceptual designs. The fuel cell module development effort comprises three coordinated tasks:

Task 1: Design of Large Cell Stacks
Task 2: Stack Fabrication
Task 3: Stack Testing

The "Fuel Conditioner Subsystem Development" task is the fourth technical task of this effort. Provision for "Management, Reporting and Documentation" is included as a fifth task.

The work accomplished during this reporting period is described at the subtask level in the following section.

II. TECHNICAL PROGRESS SUMMARY

TASK 1: DESIGN OF LARGE CELL STACKS

1.2 Stack Design

A review of the designs of Stacks 560, 561, 562 and 563 was held as part of the November progress review meeting. The major conclusions were:

1. The bipolar and bipolar/cooler plates for Stack 561 will be heat treated,
2. Acid fill Scheme 2, as originally conceived, will be used in all four stacks.

The decision to heat treat 561 was based largely on the excellent progress made in the heat treating experiments and was made possible by delays related to a disappointing flow of makeup acid through Stack 559. This decision involved heat treating assembled coolers since they were assembled prior to the design review. Based on ERC's successful experience on other programs, a very conservative cycle was selected, approved by the NASA Project Manager and was apparently successful.

The reduced flow of acid through the makeup system of Stack 559 was apparently due to details of construction of the stack and these were associated with design modifications to the original conception of Scheme 2. As part of the November progress review meeting, two plexiglass models of the acid makeup system were displayed. A glycerine solution that had room temperature viscosity and surface tension nearly equal to those of the acid at the stack operating temperature was fed to the models. The observed flow patterns indicated that the design modifications were not necessary to insure contact of the acid with the matrix. Since elimination of these modifications simplifies stack assembly and permits operation of the stack with the acid channels above or below the cells, a decision was made to return to the original concept.

Other design features of the next four stacks (560 through 563) are:

1. An improved acid feed tube which eliminates the possibility of leakage into the space between the end plate and the compression plate.
2. The use of crossed compression bars* on the 23 cell stacks (561, 562 and 563).

A document describing these features in more detail and the fabrication and assembly procedures and the test plans for these stacks was prepared and submitted to the NASA Project Manager.

1.3 Full Scale Module Designs

1.3.1 Material Characterization of Repeating Components

The following summarizes and rationalizes the work done to determine the thermal and mechanical properties of the cell materials. This information is needed to evaluate new ideas, calculate contact forces between components, calculate the differential motion between stack and manifold and the resulting shear forces applied to the stack-to-manifold seal. Height change measurements, such as those of an 80 cell stack reported in the 4th Quarterly Report, pertain to a unique total system and they cannot be generalized.

The benefit derived from knowing the basic properties of these materials is illustrated in the following example. A cross-section through a hypothetical cell before and after compression is shown in Figure 1. The shims shown in this design seal the edges of the fuel cell to prevent intermixing of the reactant gases, act as a mechanical stop to limit the contact force on the anode-matrix-cathode composite and its protrusion into the gas flow channels, and electrically insulate

*Described in the 4th Quarterly Report.

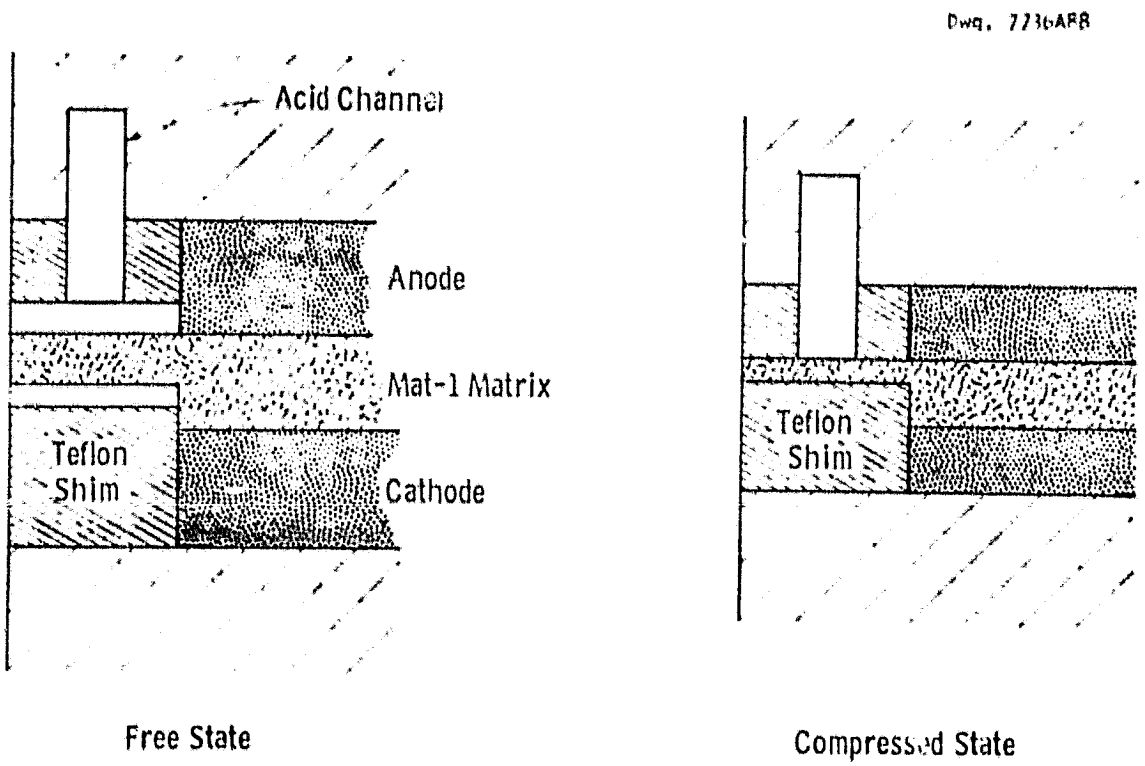

Fig. 1 —Cross section through a hypothetical phosphoric acid fuel cell before and after applying a compressive load

adjacent cells. If the thermal and mechanical properties of the repeating components are not known, the correct thickness of these shims must be determined by trial and error on full size cells in multi-cell stacks.

During the development phase of a project, it is good engineering practice to design components so they can be readily changed. This permits the evaluation of different configurations, before committing to costly and long-lead time tooling (for example, the purchase of a mold for the bipolar plates). Once the development has been completed, it is equally good engineering practice to review and simplify the design. Often, the functions of several components are combined into one component or parts are eliminated and product cost is reduced. Thus, the developmental design in Figure 1 can be simplified by eliminating at least one of the shims and incorporating the shim's mechanical stop function into the design of the bipolar plate. This can be accomplished by increasing the thickness of the bipolar plate in the region occupied by the upper shim, which incorporates a long and narrow opening, conforming to the acid channel. Moreover, the thickness of the lower shim may be reduced by increasing the thickness of the bipolar plate (as in the case of the upper shim) or it may be replaced by a cost of insulating material (such as a liquid fluoroelastomer) on the raised portion of the bipolar plate. Obviously, such a final design would simplify the assembly of the fuel cells and reduce the cost of the stack. The availability of the basic thermal and mechanical properties will permit calculating and analyzing the dimensions of the revised bipolar plates and minimize experimentation required to evaluate new ideas.

Other design calculations which require knowledge of mechanical properties are: a) the protrusion of the anode-matrix-cathode composite into the bipolar plate flow channels and b) the deformation of the stack for given applied loads.

Cyclic Tests

The first tests measured the effects of repeated cycles on sandwiches of the soft components (anode-matrix-cathode) of the cell. The sandwiches were compressed in a fixture with flat faces as shown in Figure 2. The conditions and results of the tests are summarized in Table I. Figure 3 depicts the sixth through the ninth cycles of a typical test article. The results are of sufficient uniformity to permit their use as mechanical property data over the applied-force range. The graph of the first test cycle of a similar article (Figure 4) illustrates a quite different material behavior. The distance between the graph's start and end points (hysteresis loop) is much larger than in subsequent test cycles. The congruence of the load vs. deformation plots shown in Figure 3 indicates that the mechanical property changes essentially have taken place by the sixth cycle for the applied-force range over which these tests were performed. For the tenth compression cycle of another similar article, the applied force range was increased from 360 to 890 Newtons (80 to 200 lbs.)* and the load vs. deformation plot with a kink depicted in Figure 5 was obtained. While the plot over the initial range (0 to 360 Newtons (80 lbs.)) is curvilinear, it is almost a straight line for loads exceeding 450 Newtons (100 lbs.).

The 450 N load corresponds to a stress of 620 kPa (90 psi) on the 7.26 cm^2 specimen. Thus it appears that for stresses over 620 kPa (90 psi), the composite was sufficiently compacted to behave like a solid. As approximated by the tangent to the linear portion of the curve, the modulus of elasticity is 29 MPa (4,100 psi) at room temperature (line 5 in Table I).

*NOTE: The test data was originally obtained in English units and then converted to the metric system. The conversion was rounded off to prevent implication of greater precision.

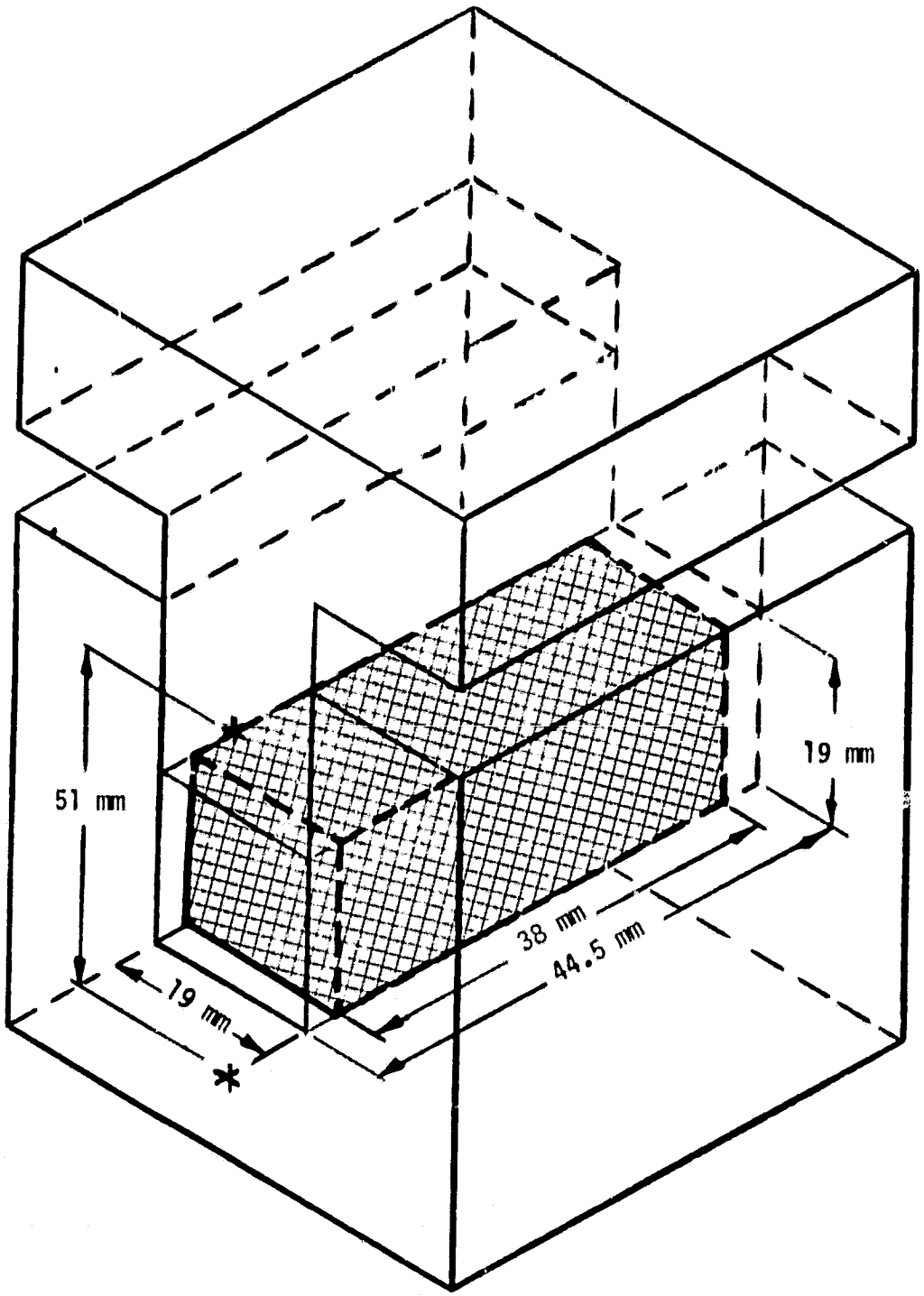

Figure 2

TEST FIXTURE FOR DETERMINING LOAD/DEFORMATION DATA

TABLE I—SUMMARY OF LOAD VERSUS DEFORMATION COMPRESSION TEST DATA

Description of Test Article	Contact Surface Topography	Technicians: Identity	Technicians: Ref. Test #	A_N Area to Which the Load Has Been Applied: Nominal mm^2	A_E Area to Which the Load Has Been Applied: Effective mm^2	P Maximum Applied Load Newtons	$\sigma = \frac{P}{A_E}$ Stress = Load ÷ Effective Area Kilopascals	Number of Test Cycles: Performed	Number of Test Cycles: Averaged are the Last	N Number of Specimen Per Test Article or Equivalent	L Height of Test Article mm	Data Points Locally Approximated by	ΔL Change in Height of Test Article mm	ΔL Change in Height Determined by Linear Approximation for the Given Load Range mm	$\varepsilon = \frac{\Delta L}{L}$ Strain mm/mm	T Temperature at Which Tests Were Performed °C	$E = \frac{\sigma}{\varepsilon}$ Modulus of Elasticity Kilo-Pascals $\times 10^3$	Lbs/in^2 $\times 10^3$
1. Anode-Matrix-Cathode	Flat	T-1	1	726	Same	360	490	1	1	14	18.87	Chord	.508	.508	.027	25	18	2.6
2. Anode-Matrix-Cathode	Ribbed	T-2	2	645	103	70	690	1	1	1	1.40	Chord	.081	.081	.059	25	12	1.7
3. Anode-Matrix-Cathode	Flat	T-1	2	726	Same	360	490	12	3	14	19.25	Tangent	.272	.211	.011	25	45	6.5
4. Anode-Matrix-Cathode	Ribbed	T-2	2	645	103	140	1380	1	1	1	1.40	Chord	.023	N.A.	N.A.	25	N.A.	
5. Anode-Matrix-Cathode	Flat	T-1	3	726	Same	890	1230	10	1	14	18.87	Tangent	.701	.812	.043	25	29	4.1
6. Anode-Matrix-Cathode	Ribbed	T-2	2	645	103	890	8610	1	1	1	1.40	Tangent	.615	.467	.340	25	25	3.7
7. Anode-Matrix-Cathode	Ribbed	T-2	13	645	103	890	8610	1	1	4	5.58	Tangent	2.057	1.727	.310	25	28	4.0
8. Anode-Matrix-Cathode	Flat	T-1	5	726	Same	360	490	9	3	14	18.54	Tangent	.424	.320	.017	200	29	4.1
9. Anode-Matrix-Cathode	Flat	T-1	6	726	Same	890	1230	16	1	14	18.54	Tangent	1.041	1.260	.067	200	18	2.7
10. Anode-Matrix-Cathode	Ribbed	T-1	16	41	0.65	17	2580	1	1	6	6.38	Chord	.965	.965	.115	200	22	3.3
11. Mat-1, Matrix	Flat	T-1	8	726	Same	360	490	9	3	84	18.72	Tangent	.305	.264	.014	25	35	5.0
12. Mat-1, Matrix	Flat	T-1	9	726	Same	890	1230	10	1	84	18.72	Tangent	.991	1.295	.069	25	18	2.6
13. Mat-1, Matrix	Flat	T-1	11	726	Same	360	490	15	3	84	17.60	Tangent	.305	.312	.018	200	27	4.0
14. Mat-1, Matrix	Flat	T-1	12	726	Same	890	1230	16	1	84	17.60	Tangent	1.092	1.500	.085	200	15	2.1
15. Bipolar Plate	Ribbed	T-2	14	645	103	890	8610	1	1	5	18.82	Tangent	.254	.152	.008	25	1,000	150
16. Bipolar Plate	Flat	T-1	—	36	Same	2,000	56500	6	2	4.77	17.93	Tangent	.048	.048	.003	25	21,000	3,000
17. Bipolar Plate	Flat	T-1	—	36	Same	2,000	56500	7	2	4.77	17.93	Tangent	.122	.122	.007	200	8,000	1,200

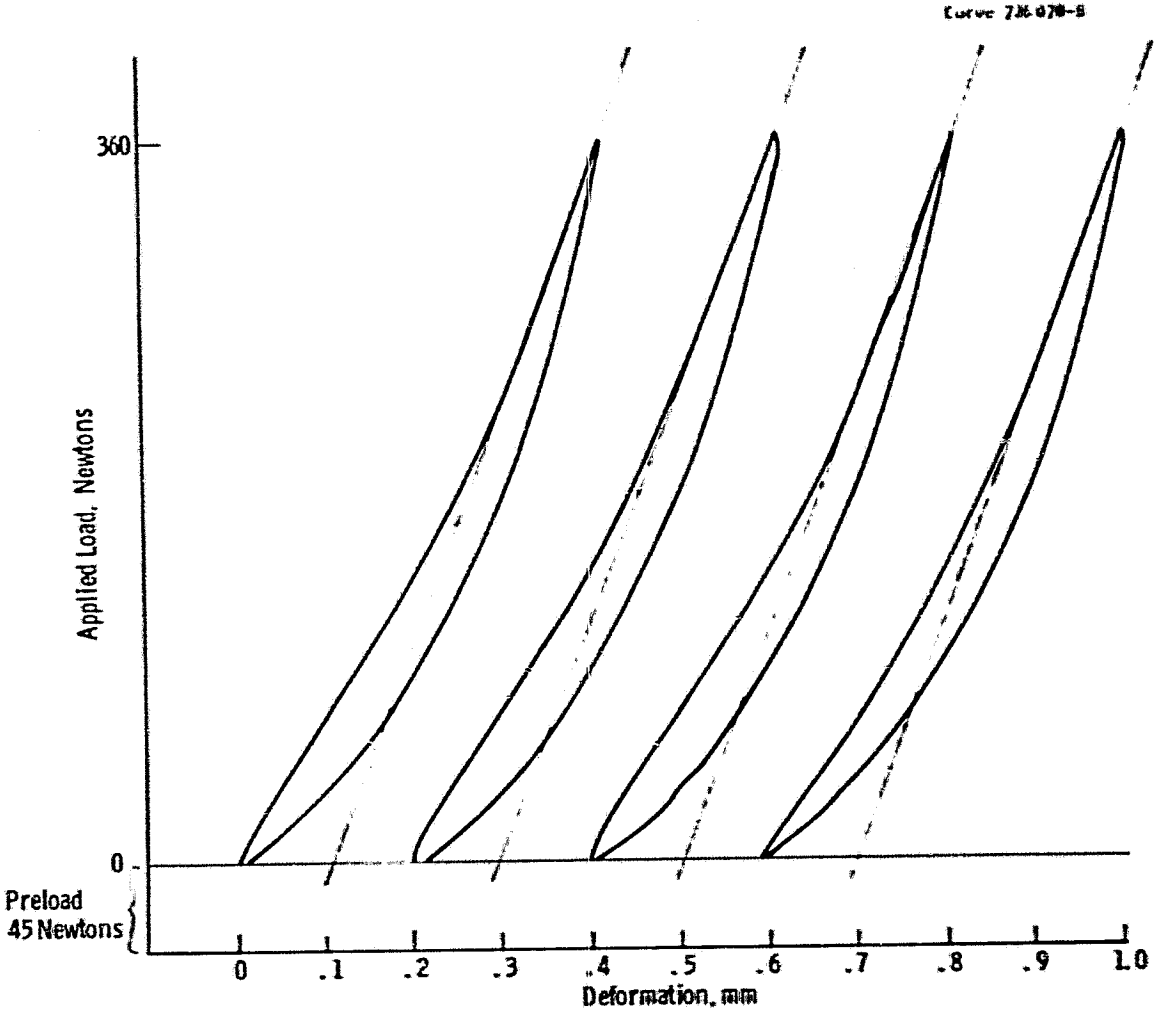

Fig. 3 —Load versus deformation plot 6th, 7th, 8th and 9th compression cycle, anode-Mat-I matrix-cathode composite. Height of Test Article: 18.54 mm, Temperature: 200°C

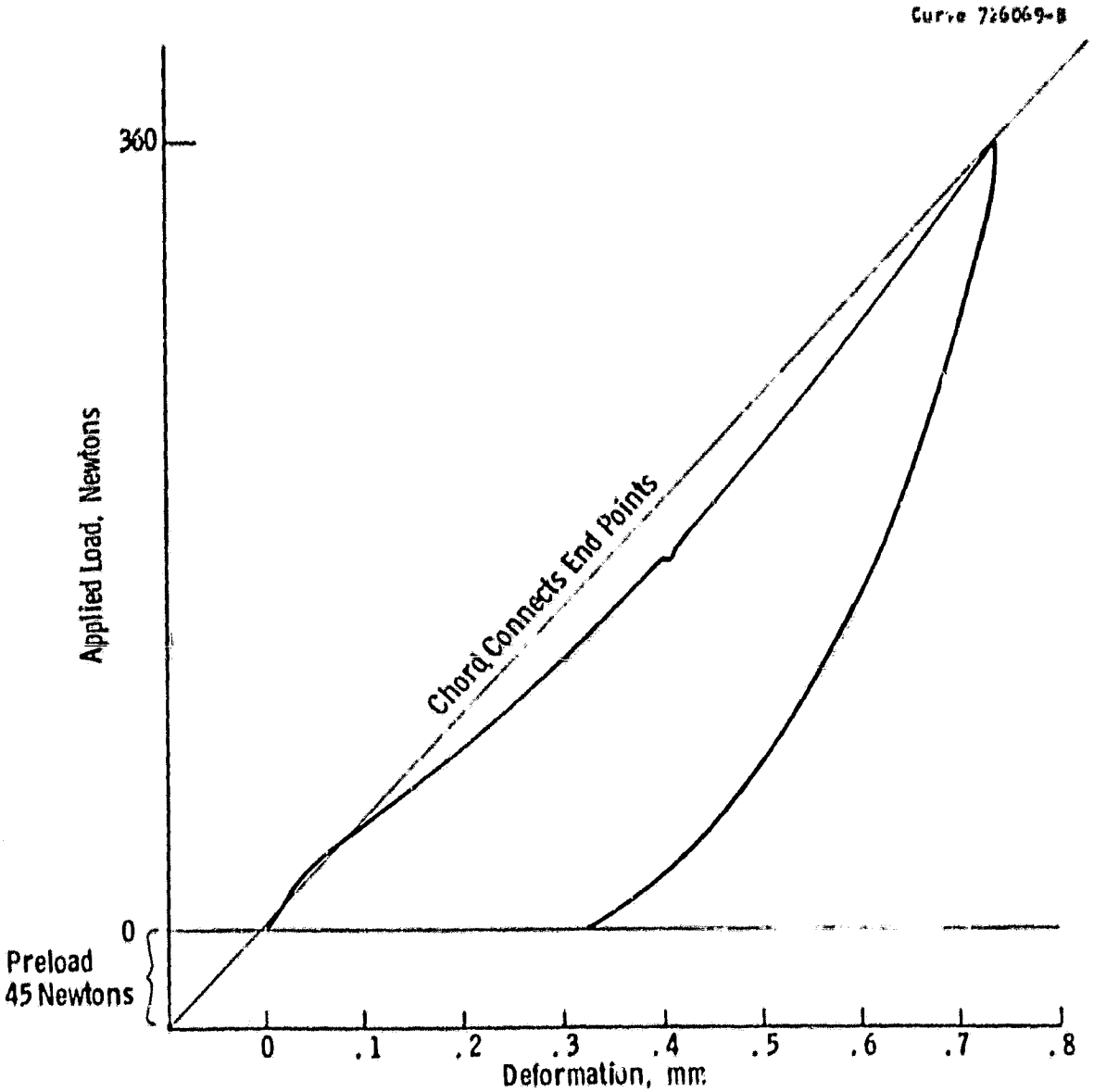

Fig. 4 —Load versus deformation plot 1st compression cycle, anode-Mat-I matrix - cathode composite. Temperature: 200°C. Height of Test Article: 18.54 mm

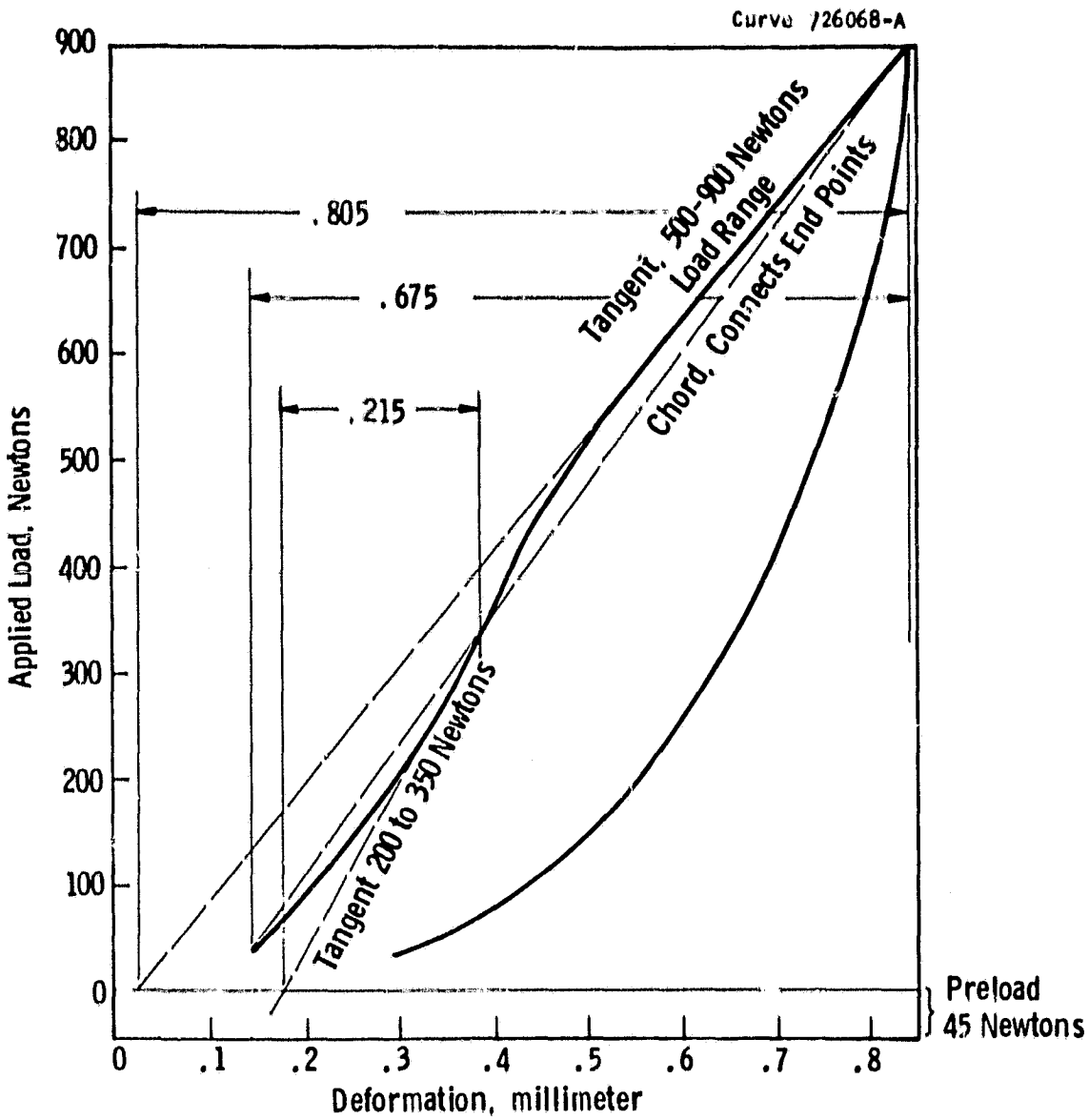

Fig. 5 —Load versus deformation, test #3
Test article height 18.58 mm
Test performed at room temperature 25°C

Ribbed Tests

Compression tests of anode-matrix-cathode composite positioned between two bipolar plates with the flow channels perpendicular to each other were also made. In these tests the applied force was 900 Newtons (200 lbs.), but, because of the bipolar plate's flow channels, the contact area was 16% of the nominal area. Consequently, the maximum stress to which the soft composite was subjected was 8.5 MPa (1,250 psi). The modulus of elasticity is 28 MPa (4,000 psi).

Additional tests of this configuration performed at 200°C (the stack's operating temperature) had results comparable with those obtained at room temperature.

Comparison of "Sandwich" Test Results

The mechanical properties measured by the two sets of tests of "sandwiches" are summarized in Table I. As indicated in the figures, straight lines were fitted to the data points of the load versus deformation graph for given load ranges. Usually the line is a tangent. However, in some cases where only the end points are known, the straight line is a chord connecting the maximum and minimum applied-load point. The chord approximation gives a linear function over the entire load range at a sacrifice in accuracy. The tangent gives a linear function over a more limited load range, but tends to be more representative for the given load range. Figure 5 illustrates the different methods. The summary of the data in Table I indicates which method has been used for calculating the modulus of elasticity.

As indicated previously, many compression cycles must be performed before reproducible plots are obtained at low loads. For the sake of completeness, the modulus of elasticity "E" for the first compression cycles are shown on lines 1 and 2 for flat surfaces and ribbed bipolar plates, respectively. The ribs were oriented at right angles to each other so that the contacting surface was approximately 16% of the nominal surface. A stack of 14 sandwiches was used for the

flat contact surface listed while one sandwich was used for the ribbed contact surface. The moduli, 18 and 12 MPa (2600 and 1700 psi), show reasonable agreement, considering the differences in test articles, that the tests were carried out at low loads and that the slopes used were the chords between beginning and end points. As shown in lines 5, 6 and 7, when the applied load was increased to 890 Newtons (200 lbs.) and the data points were fitted by a tangent, the agreement among the test data was much better (i.e., 29, 25 and 28 MPa (4100, 3700 and 4000 psi)).

We, therefore, conclude that for the anode-matrix-cathode composite, a modulus of elasticity of approximately 26 MPa (3750 psi) is applicable over a wide range of pressures and temperatures. Moreover, the modulus is not too sensitive to differences of the contact surfaces. This is a very desirable result, since new flow channel dimensions or configurations can be readily incorporated without fear of effecting the mechanical properties of the anode-matrix-cathode composite.

Matrix

The mechanical properties of the Mat-I matrix by itself were measured since the matrix extends over the inactive areas boxes of the bipolar plates, see Figure 1. While the modulus of elasticity for the Mat-I matrix does not exhibit a great sensitivity to temperature changes ranging from room temperature to 200°C, it reduces to approximately one half of its value when the pressure is increased from 490 Kilo pascals (70 psi) to 1230 Kilo pascals (180 psi) (Table I). Since the inactive area of the bipolar plate is only about 10% of the total nominal area (1300 cm^2 or 204 in^2) and the nominal pressure over the total area is 400 Kilo pascals (60 psi), there is a great likelihood that the local pressure in the inactive area exceeds 500 Kilo pascals (80 psi). Thus the lower modulus, applicable over the upper load range, should be used.

Bipolar Plates

The non-heat-treated bipolar plates have a modulus of 1 GPa (150,000 psi). After heat treatment, the modulus increased to 21 GPa (3 million psi) at room temperature. This reduced to approximately one half of its value at 200°C (lines 15 and 17 of Table I). The large difference between the heat treated and non-heat-treated material can probably be attributed to the reduced resin content of the heat treated material.

Conclusions

Based on these tests, the stack contraction (and, therefore, the shear forces to which the stack-to-manifold seals are subjected) is primarily a function of the applied load range. The modulus of elasticity ranges from 18 MPa (2600 psi) to 28 MPa (4100 psi) for an applied stress ranging from 350 to 8500 kPa (50 to 1250 psi) and a temperature ranging from 25 to 200°C. The only caveat is that allowance must be made for the initial deformation which occurs during the first few compression cycles at the lower applied load range. One way to accommodate this is to assemble the stack without manifolds. Then subject the stack to, say, 15 compression cycles and 200°C and only thereafter attach the manifold-to-stack seals and manifolds. Most of the deformation will have taken place, the repeating components will have mechanically stabilized and the shear stresses on the manifold-to-stack seals will have been greatly reduced.

Due to the very high moduli of the bipolar plate materials (particularly the heat treated version), the fuel cell stack contraction results from the deformation of the matrix-shim and anode-matrix-cathode composites. In addition we find that at effective pressures in excess of 700 Kilo pascals (100 psi), the matrix as well as the anode-matrix-cathode composite appear to deform permanently. These materials behave structurally, similar to corrugated cardboard, although not as extreme. When a flat piece of corrugated cardboard is compressed between two

flat blocks, it will return to its original thickness as long as the corrugations are not permanently deformed. This is the behavior of the anode-matrix-cathode composite, observed at effective pressures from 400 to 600 kPa (60 to 80 psi). However, if the pressure the corrugated cardboard is subjected to is sufficient to crush the corrugations and the air space between the face sheets is eliminated or greatly reduced, the crushed corrugated board is permanently deformed and then behaves like solid cardboard. That is, it still has elastic properties, but its behavior has changed from a soft to a stiff spring. Since the effective contact area of the bipolar plate is much smaller than its nominal area, it is very likely that at least the matrix in the inactive area is crushed when a nominal load of 400 kPa (60 psi) is applied to the stack.

This concludes the task for evaluating the thermal and mechanical properties of the repeating components. Mathematical models have been and will continue to be developed to calculate the pressure distribution over the fuel cell surface and the expected height changes, resulting from this pressure distribution. Depending on the contact area, different gas flow channel configurations are expected to result in greater or smaller height changes, which must be accommodated by stack-to-manifold seals. We now have the tools to calculate these changes.

1.3.2 Manifold Design and Concepts

The manifold's major function is to distribute the gas flow evenly over the height of the fuel cell stack. At first glance, it appears that this is not very difficult. There are, however, several factors to be considered. First, the manifold must withstand a 200°C temperature continually. Second, it has to be corrosion resistant because of its exposure to a phosphoric acid environment. Third, it should reasonably match the thermal expansion characteristics of the fuel cell stack, in order to minimize the shear forces on the stack-to-manifold seal once the cell material properties have stabilized. Finally, its surface must be an electric insulator to prevent electric arcing or

shorting of the stack. For short stacks, consisting of a small number of fuel cells, the electric arcing problem is minor because of the low voltages. As the number of cells per stack increases, however, and the voltage increases proportionally, arcing or electric shorting can become a major problem. Thus, various manifold design concepts, materials and their costs to satisfy all of these requirements are being evaluated.

One of the current design concepts interposes a frame-shaped insulator between a metal manifold and the stack to prevent electrical shorting. This concept is shown in Figure 6. Examination of this design approach leads to the question: Provided a material exists from which the frame-shaped insulator can be fabricated, why not use this same material for fabricating the manifold and eliminate the frame and the second set of gasket seals. Two such manifold designs are being explored; one made of an insulating material, the other made of sheet metal coated with insulation.

Non-Metal Manifolds

The selection of candidate materials from a Westinghouse material data base was completed and the thermal aging properties of the selected candidate materials were examined. In-use operation over long times provides the most desirable aging data. However, this approach is much too time-consuming to be practical. Hence, the thermal-aging properties of insulating materials have been estimated from Arrhenius plots. The aging properties are based on the length of time a material can continually tolerate a given temperature and retain 50% of its mechanical strength. A typical Arrhenius Plot for Bakelite Polysulfone is shown in Figure 7.

Only two of the eight original candidate materials are still under consideration. These are Ryton (Polyphenylene Sulfide, Phillips Petroleum Co.) and Epoxy. Teflon has been eliminated because of its very high cost and lack of sufficient mechanical strength. Silicone is too difficult to mold in large sizes. The rest of the materials were ruled out because their average life at 190°C was less than one year.

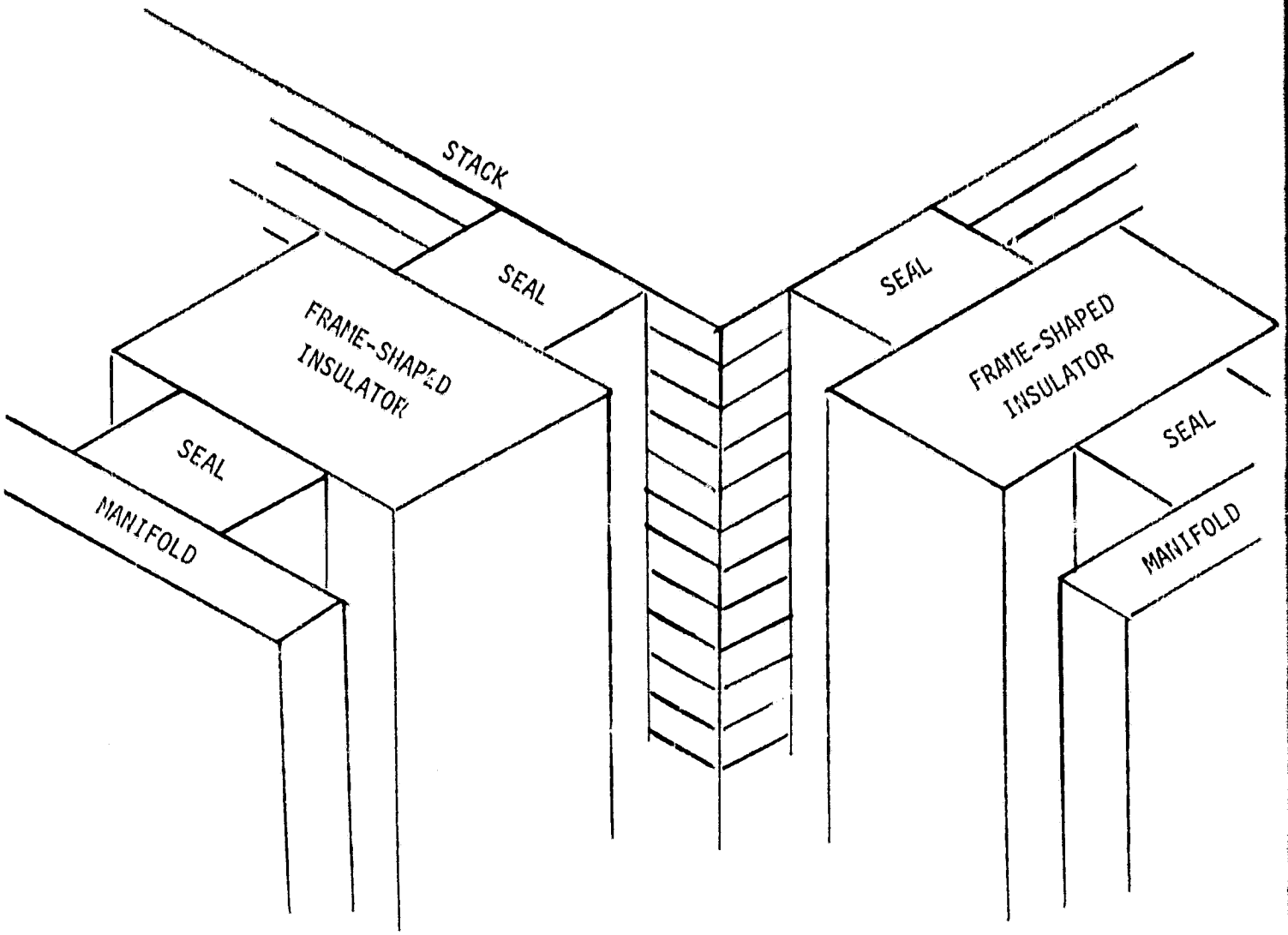

FIGURE 6

MANIFOLD DESIGN CONCEPT WITH A
FRAME-SHAPED INSULATOR INTERPOSED
BETWEEN METAL MANIFOLDS AND STACK

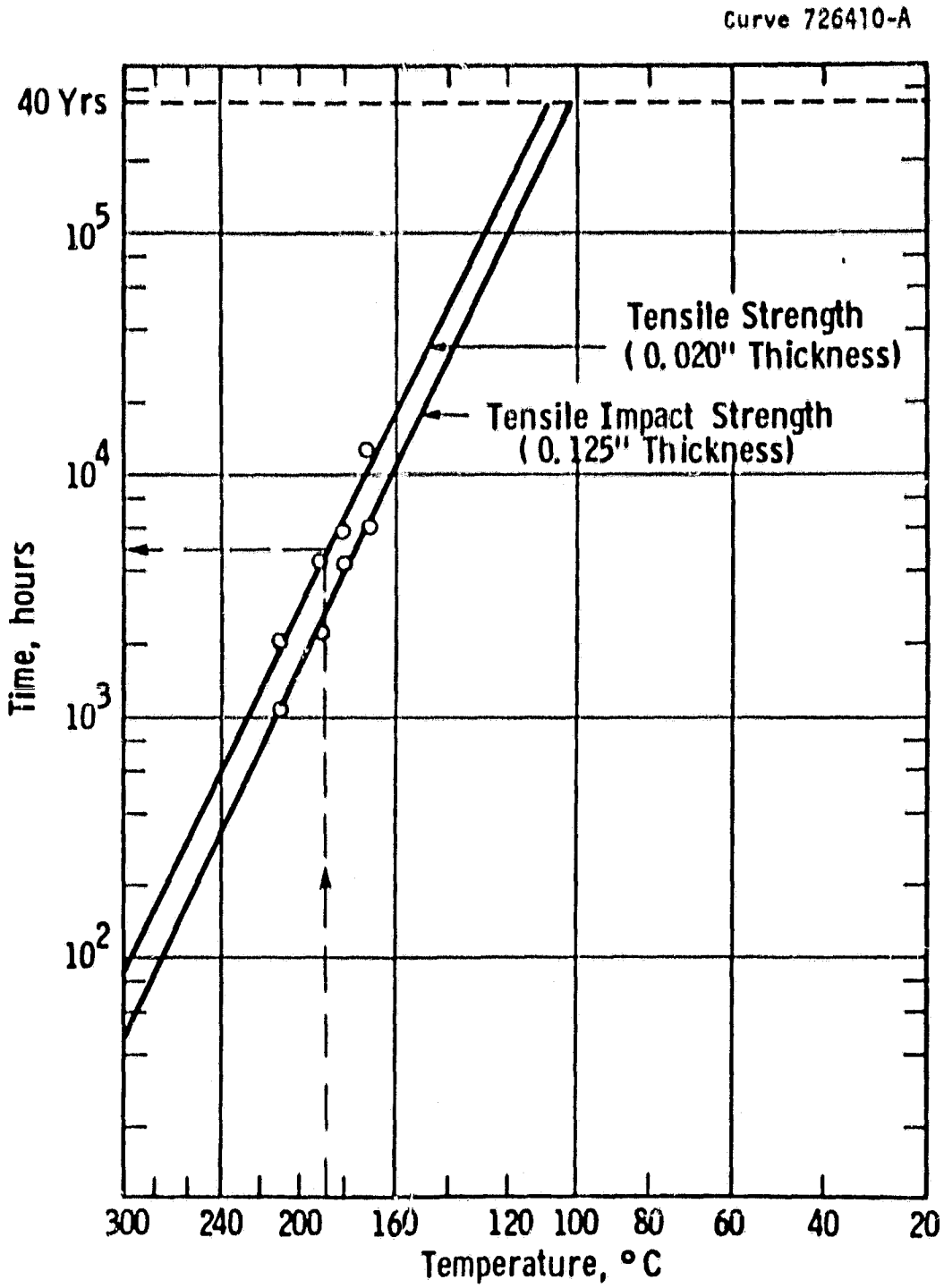

Fig. 7— Arrhenius plots at 50% retention of properties for Bakelite Polysulfone P-1700

Metal Manifolds with Protective Coatings

The thermal aging properties of protective coatings are similar to those of the solid molded material but the mechanical strength requirements of the protective coatings are less severe. Figure 8 illustrates the relative material costs for several 0.8 mm (0.032 inch) thick sheet metals with protective coatings. For reference purposes, bare, uncoated 316 stainless steel ($1.50/pound), nickel, and 0.32 mm (0.125 inch) thick Ryton (Polyphenylenesulfide) have been shown. Only FEP (Tetrafluoroethylene-hexafluoropropylene) coated carbon steel has a reasonable cost of approximately three dollars per Kilowatt. This is for a 0.25 mm (0.010 inch) thick coat on 0.8 mm (0.032 inch) thick carbon steel. One problem with all the Teflon coatings is their lack of long term adherence to metals. Because of their high cost, PFA and PTFE coated steels have been eliminated.

Since conventional 316 stainless steel, commonly used for fabricating chemical processing equipment, corrodes 9 mm per year on exposure to 70% phosphoric at 140°C, we contacted Jessop Steel Company (stainless steel manufacturer). They make a special stainless steel (JS 700) which, under the same conditions, corrodes only 0.3 mm per year. The cost, however, is $3.72/pound versus $1.50 for 316.

The evaluation and cost tradeoffs of alternate manifold materials will be continued during the next quarter.

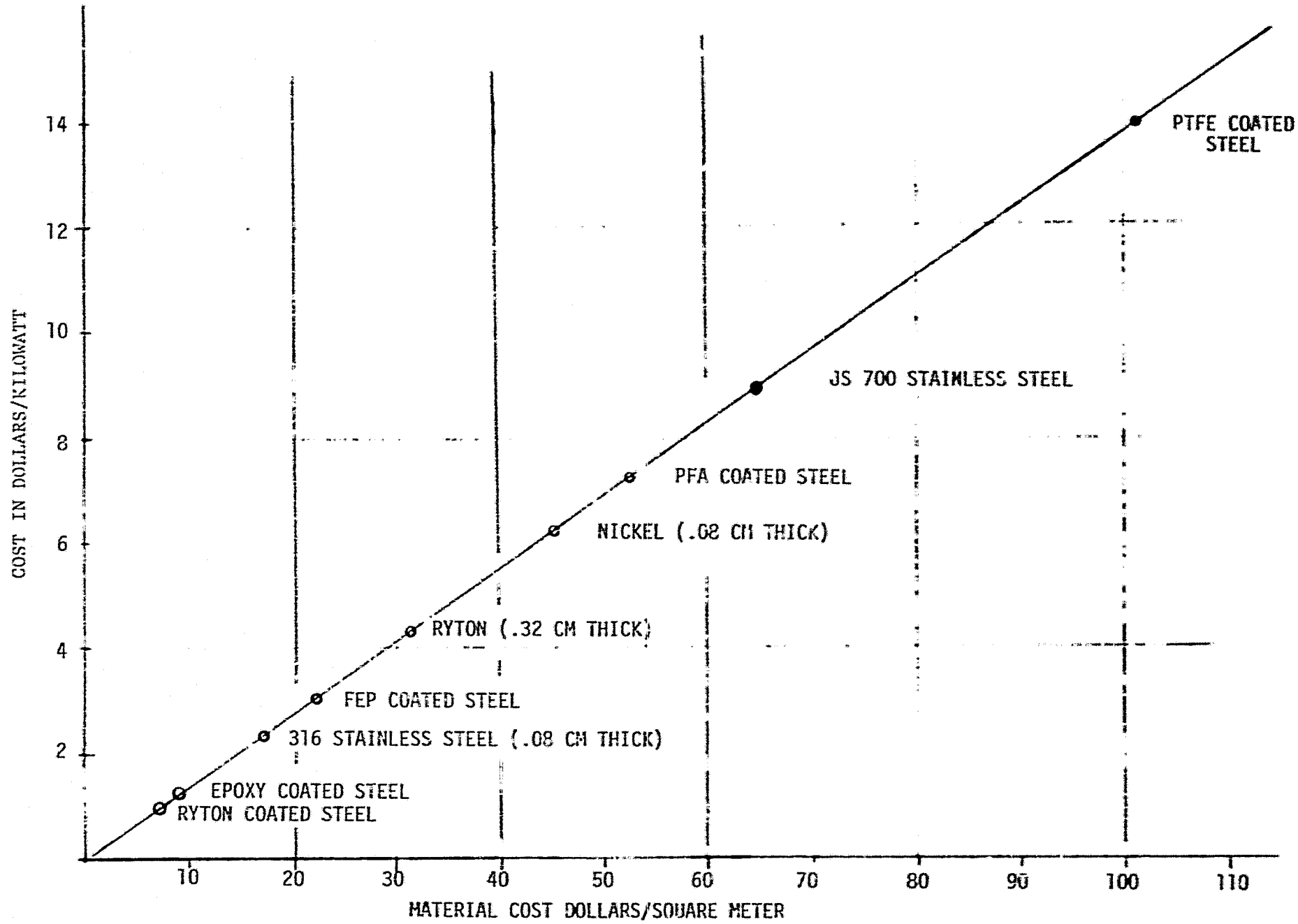

Figure 8 - COST ESTIMATES FOR FUEL CELL MANIFOLDS
FUEL, OXYGEN AND COOLING AIR
300 CELL UNIT

TASK 2: STACK FABRICATION

2.1 Methods and Approach

Heat-Treatment

Experiments were performed to establish heat-treatment cycles for the MK-2 design bipolar plates and for thick bipolar/cooling plates with the innovative cooling channel configuration. The incorrectly machined plates discussed in previous reports were used for these experiments. The cycle was used for heat-treatment of plates for stacks 560 (5-cell, MK-2) and 561 (23-cell, MK-1).

Cooling Plate Assembly

To evaluate the integrity of assembled coolers, compression and thermal cycling experiments were performed on one nonheat-treated straight through cooler.* After ten decompression-compression cycles (∿1 to 414 kPa) and three heating-cooling cycles (∿177 to 25°C), the plates remained glued together, the edge seal remained intact and cooler resistance** showed no significant change, as detailed in Table II.

Tests were also made to determine any poisoning effect the bonding material used for cooling plate assembly might have on the cells.

2.2 Simulated Stack Fabrication

2.2.1 Stack 560 (5-cell, MK-2 design)

As reported in the 4th Quarterly Report, a number of blank bipolar plates were molded, leak tested and sent to the vendor for machining. Fabrication of the electrochemical cell components (matrices

*Assembled according to the procedure in the 4th Quarterly Report.

**Measured as described in the 4th Quarterly Report.

TABLE II

THE EFFECT OF THERMAL AND COMPRESSION LOAD CYCLING ON COOLING PLATE ASSEMBLY RESISTANCE*

STAGE OF ASSEMBLY	RESISTANCE, mΩ, at Voltage Lead Position							
	1	2	3	4	5	6	7	8
1. Sanded and cleaned faces of cooling halves	0.85	0.96	1.03	0.77	1.04	0.98	1.09	0.80
2. Plates assembled and cemented (414 kPa)	0.12	0.15	0.42	0.28	0.59	0.33	0.09	0.06
3. After assembled plates underwent 10 decompression-compression cycles (414 kPa)	0.13	0.17	0.37	0.30	0.27	0.34	0.20	0.21
4. After 3 heating (177°C) & cooling (25°C) cycles.	0.12	0.23	0.58	0.38	0.33	0.38	0.22	0.20

* i = 10 amps

and electrodes) was also initiated during the 4th quarter and completed at the beginning of this quarter. The machined bipolar/end plates were received in November and they were examined, heat-treated and leak tested again to insure integrity of the plates. The cell subassemblies were completed at the beginning of December. Stack assembly will be started early in the next quarter.

2.3 Short Stack Fabrication

2.3.1 Stack 561 (23 cell, MK-1 design)

Fabrication of all cell components and coolers was completed during the previous quarter.* Stack assembly was postponed to make maximum use of the information gathered on Stack 559 which was also a 23 cell, MK-1 stack.

As described under Task 1, a decision was made to use heat-treated plates in Stack 561. The bipolar plates and previously assembled cooling plates were heat-treated along with the plates for Stack 560. The required stack auxiliary hardware (compression plates, Haysite insulator, manifolds, etc.) were fabricated and cell subassemblies completed. The stack will be assembled in January.

2.3.2 Stack 562 (23 cell, MK-2 design)

The electrodes and matrices for Stack 562 were completed in early October, along with the components for Stacks 560, 561 and 563. A partial shipment of machined plates for Stack 562 (bipolar plates and cooling half plates) was received in November. These plates were inspected and leak-tested. When the balance of the machined plates are received, they will be inspected and the complete set will be heat treated.

*As discussed in the 4th Quarterly Report.

2.3.3 Stack 563 (2 cell, MK-1 design)

The fabrication of all electrochemical components and bipolar plates was completed during this quarter. The blank cooling half plates were molded and sent to the machine shop on November 24. The cooling channel design for this stack will be finalized after analysis of the Stack 561 temperature distribution data.

TASK 3. STACK TESTING

3.3 Short Stack Testing

Stack 559 (23-cell, MK-1 design)

Pretesting

The stack was compressed to 340 kPa and acid addition started. Some acid was weeping from the edges of matrices and the acid feed rate was disappointingly low. To determine the reason for the slow acid feed, holes were drilled into the acid channels and gas tests were conducted. These tests indicated no singular blockage but rather generally restricted flow throughout the acid path. However, since the matrices appeared adequately filled, the stack compression was increased to 410 kPa and testing continued. This increase effectively reduced the acid weepage to a negligible level.

The stack was pretested at ∿100 mA/cm^2 for 62 hours at ERC before shipment to Westinghouse. Its pretest history is shown in Figure 9. The time averaged performance was ∿0.57 V/cell which is reasonable for this kind of build. Approximately one cc/cell of acid was added to the stack just before its shipment to Westinghouse.

OS/IES Loop Testing

Stack 559 was delivered to Westinghouse the last week in October and the first test was made on October 28. A representative from ERC was present to witness our startup and test procedures to insure that they conformed to those used at ERC. The test conditions were adjusted to agree with an ERC test made five days earlier. The measured data agreed very closely for this duplicate test. Thus we are confident that the Westinghouse test procedure does duplicate ERC results and that the stack was not damaged during shipment.

Following the duplicate test, a series of tests were made to study the following:

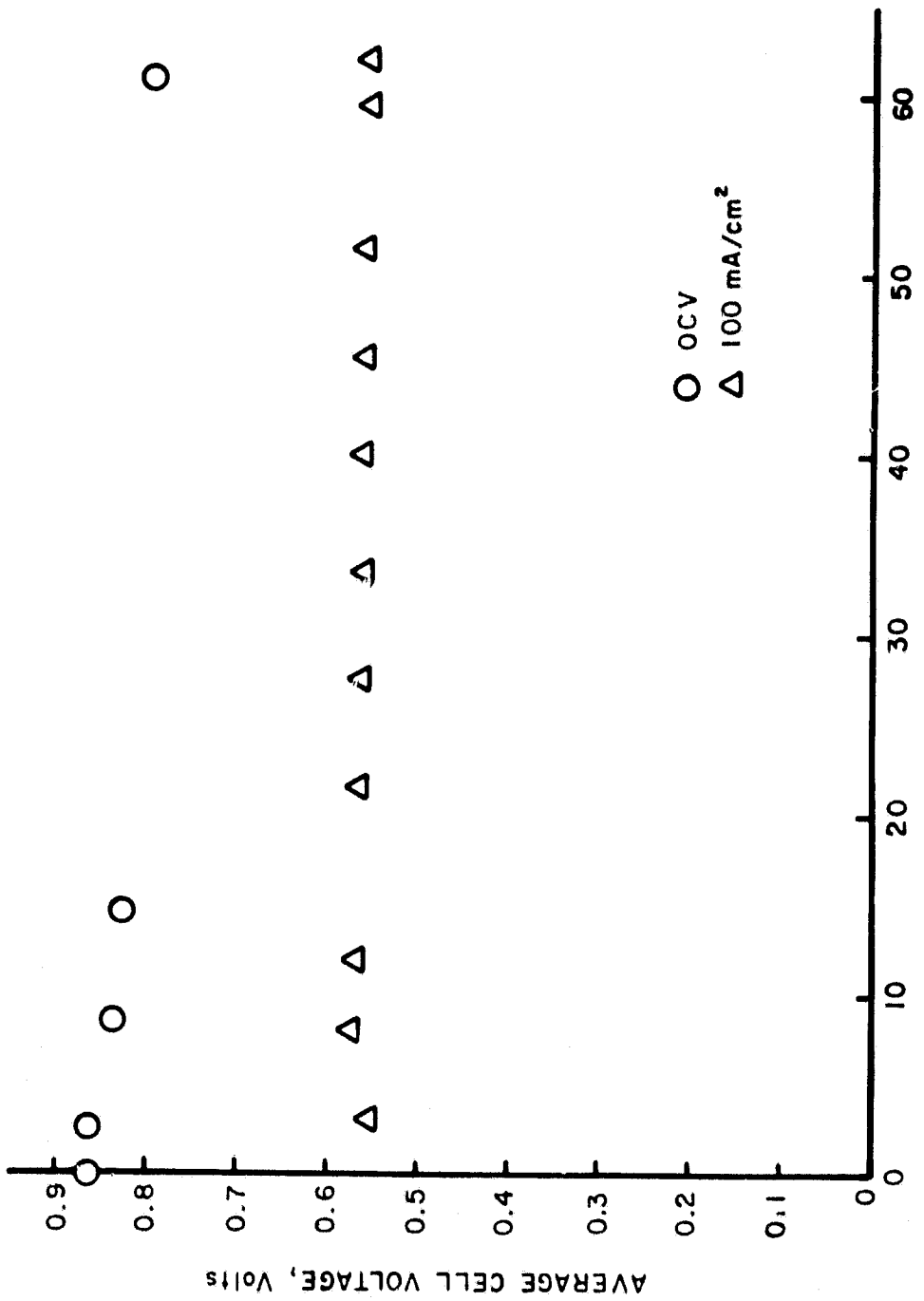

FIGURE 9 STACK 559 PERFORMANCE HISTORY

a) Temperature uniformity of the stack to assess the effectiveness of the cooling plate design.
b) Stack performance at current densities of 50, 100 and 150 mA/cm^2.
c) The effect of makeup air flow on stack performance.
d) The influence of mean plate temperature on stack performance.
e) The effect of total stack flow on temperature uniformity and stack performance.
f) The effect on temperature distribution of blocking two cooling channels per cooling plate, near the hydrogen exit edge of the stack.

Table III summarizes the ERC test and 12 steady state tests conducted at Westinghouse. The tabulated data includes fuel composition, fuel utilization, fuel inlet temperature, makeup air flow, air inlet temperature, air temperature, and temperature uniformity. These results are discussed in the following subsections. For all tests, the remaining dry fuel mole fraction was CO_2. The dry fuel mixture was humidified at room temperature for all tests except 5 and 6. Tests 1 and 2 were conducted without external thermal insulation. The stack was insulated with 5 cm (2 in.) fiberglass for all other tests.

Temperature Distribution

Stack 559 is a 23 cell digas cooled stack using 30.5 cm (12 in.) by 43.2 cm (17 in.) bipolar plates with an active area of approximately 1160 cm^2 (180 in^2). Process and cooling air flow in the 30.5 cm direction and fuel flows at right angles in the 43.2 cm direction. Bipolar/cooling plates are located after cells 4, 9, 14 and 19. Cell 12 is the middle cell of the stack and is located midway between the middle two cooling plates. The stack contained four rows of six thermocouples. The six thermocouples in each row were equally spaced in the air flow direction with the first and last thermocouples

TABLE III

SUMMARY OF STACK 559 TEST DATA

Test	Current Density, mA/cm^2	Volts/ Cell, V	Average Temp., °C	Maximum Temp., °C	Peak to Average Gradient, °C	Fuel Utilization	Dry H_2 Mole Fraction	Fuel Inlet Temp., °C	Makeup Air, Stoichs	Air Inlet Temp., °C	Air Temp. Rise, °C
1*	91.4	.555	161.6	175.0	13.4	.66	1.00	112	10.	124	39.0
2	87.2	.563	--	177.0	--	.62	1.00	106	10.	121	37.0
3	98.3	.539	172.7	181.0	8.3	.42	.75	112	4.3	121	50.5
4	97.9	.534	173.1	183.5	9.4	.64	.75	112	4.3	119	52.8
5	94.1	.514	171.6	179.5	9.1	.62	.77	104	2.0	121	49.4
6	93.8	.511	172.1	181.9	9.8	.67	.76	110	2.0	121	50.0
7	52.8	.567	178.1	184.7	6.6	.38	.74	113	2.0	122	53.4
8	145.5	.414	174.9	190.3	15.4	.47	.77	117	2.0	116	55.0
9	149.3	.427	174.6	191.6	17.0	.46	.78	116	4.0	116	55.5
10	90.3	.490	160.6	171.0	10.4	.47	.80	118	2.0	107	52.2
11	91.4	.497	160.3	168.3	8.0	.47	.79	120	2.0	130	26.7
12	92.6	.504	178.2	195.4	17.2	.51	.79	115	10.	118	61.3
13	93.7	.510	175.8	183.9	8.1	.41	.73	121	4.4	122	51.4

* ERC Test

of each row located respectively at the inlet and exit edge of the active area. The rows in cells 12 and 17 were at the center of the stack. The row in cell 11 was 5.1 cm (2 in.) from the fuel inlet edge and the row in cell 13 was 5.1 cm from the fuel exit edge. The three rows in cells 11, 12, and 13 effectively measured the temperature distribution at the center cell of the stack. The row in cell 17 duplicated the row in cell 12 between the adjacent pair of cooling plates. The average temperature of each row was obtained using the trapezoidal rule. The average stack temperature was found from the simple average of the row averages in cells 11, 12 and 13. The peak to average temperature gradient was defined as the maximum measured temperature minus the average stack temperature. This is the most meaningful gradient since material life is limited by the maximum temperature and cell performance is determined by average temperature.

The data in Table III show that excellent temperature uniformity was obtained. All tests of the insulated stack with current density between 90 and 100 mA/cm^2 produced a peak to average temperature difference less than 10°C except test 12 which had lower total air flow. A plot of the temperature distribution for a typical test is shown in Figure 10. The average temperatures in rows 11 and 12 are virtually equal and are approximately 10°C higher than in row 13.

The theoretically predicted temperature distribution for the stack is shown in Figure 10 as a dashed curve. The high slope at the air inlet was caused by localized cooling due to t' process air and by conduction to the inactive area. This slope is sensitive to plate thermal conductivity and air flow split. Test results indicated a higher air flow through the process channels or a lower thermal conductivity than used in the theory. The cooling plates were designed for an air flow split of 16 percent process and 84% cooling flow. No measurements were made to obtain the actual split. The overall temperature uniformity can be broken into two components: 1) the peak to average ΔT along a row in the coolant (air) flow direction and 2) the

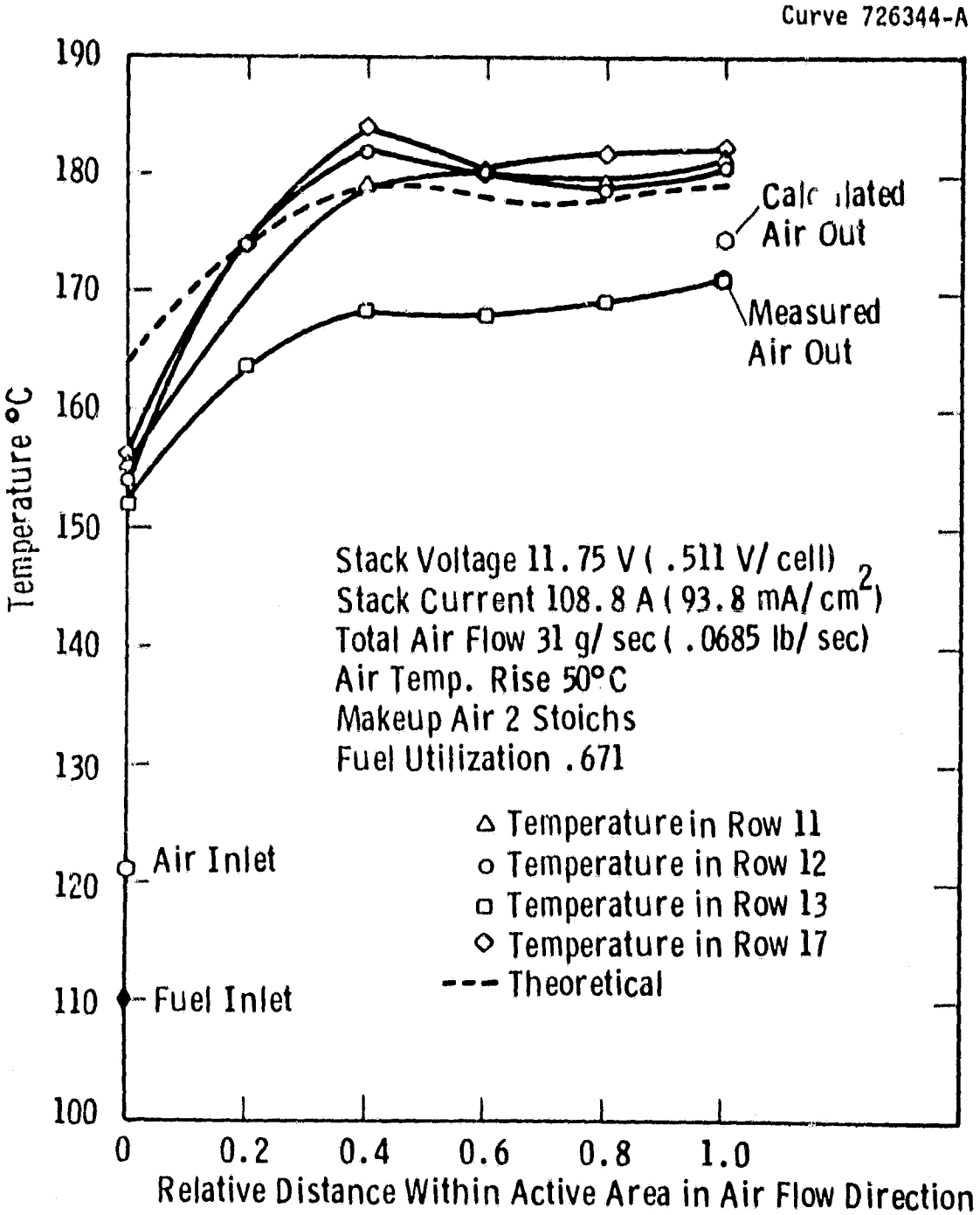

Fig. 10 — Typical temperature distribution for Stack 559

difference between the average temperature of a given row and the average of all rows (fuel flow direction). The peak to average differences (ΔT's) for the rows are given in Table IV. The theoretical ΔT was 3°C for 100 mA/cm^2 and 7°C for 150 mA/cm^2. The average temperatures of the rows are given in Table V. The spacing of cooling channels was designed to produce equal average temperatures in each row and throughout the stack. This required more closely spaced channels near the hydrogen inlet edge of the stack than at the exit edge. The test results showed a strong tendency for the hydrogen inlet edge (row 11) to overheat as fuel utilization was increased. This was initially interpreted as a stability problem. However, it was finally discovered that the closer spaced cooling channels were actually located at the hydrogen exit. Before the error was discovered, an experiment (Test 13) with reduced cooling at the fuel exit was conducted in which two cooling channels per cooling plate near the fuel exit edge were plugged. This produced an excellent balance between the three rows 11, 12 and 13 (Table V, test 13), but stack performance had deteriorated too much from initial tests to permit accurate evaluation. It is now recognized that this test only changed the cooling distribution back to the intended ratio but at a reduced amount of cooling. Row 11 was undercooled and row 13 was overcooled relative to the intended design in all other tests.

At 2 stoich makeup, the peak to average ΔT's for the stack were 6.6, 9.8 and 15.4°C for respective current densities of 53, 94 and 146 mA/cm^2. The peak to average ΔT's for row 12 were 3.4, 5.1 and 8.0 for the respective tests. Predicted values of these latter ΔT's for 50, 100 and 150 mA/cm^2 are 5, 3 and 7°C, respectively.

Effect of Total Stack Air Flow

Nearly all insulated stack tests were run with an air flow which gave a temperature rise of 50 to 55°C. One test at 26.7°C air rise (approximately double the normal flow) reduced the peak to average

TABLE IV

PEAK TO AVERAGE TEMPERATURE

DIFFERENCE WITHIN EACH ROW FOR TESTS OF TABLE I

Test	Row 11	Row 12	Row 13	Row 17
1	8.0	7.2	6.1	6.1
2	-	-	4.4	-
3	7.6	6.	5.8	6.5
4	8.8	6.2	5.4	6.0
5	7.5	5.5	4.5	5.8
6	7.6	5.1	4.9	6.1
7	5.3	3.4	2.5	3.8
8	11.5	8.0	4.7	7.9
9	13.1	7.6	5.1	8.0
10	5.9	7.5	14.8	6.7
11	5.4	4.2	10.6	5.8
12	8.9	12.0	2.9	8.2
13	9.4	6.3	6.1	6.8

TABLE V

AVERAGE TEMPERATURE OF EACH
ROW FOR TESTS IN TABLE I

Test	Row 11	Row 12	Row 13	Row 17
1	155	167.8	161.9	168.9
2	-	--	164.4	--
3	168.1	174.7	175.2	177.9
4	173.7	175.9	169.7	178.4
5	171.2	175.2	168.6	177.2
6	173.8	176.3	166.1	177.9
7	175.2	181.3	177.7	182.8
8	178.8	179.0	167.0	181.0
9	178.5	178.0	167.2	180.6
10	162.6	163.5	155.6	161.7
11	160.1	163.0	157.7	162.0
12	182.8	183.4	168.3	181.0
13	172.6	177.0	177.8	179.4

ΔT from 10.4 to 8.0°C. The performance improved 7 mV/cell due to the increased process flow at the same inlet oxygen concentration. Doubling air flow theoretically increases performance by 5 mV/cell with the 2 stoich makeup used in this test. The increased flow was not expected to make a significant change in temperature uniformity.

The Effect of Current Density and Makeup Air

Polarization curves from steady state tests at 2 and 4.3 stoich makeup air are shown in Figure 11 by circles and squares, respectively. The data shown by open circles are for mean temperatures between 171 and 178°C. The difference due to the different oxygen concentration for 2 and 4.3 stoich makeup is very close to the expected 25 mV/cell. The darkened circles are for two tests at 2 stoich makeup with mean stack temperatures of 160°C. The difference of 3 mV/°C is higher than the expected effect of 1.2 mV/°C but the tests at low temperature were performed later in the test sequence. Thus, part of the temperature sensitivity observed is due to the decay in performance which occurred during the test period. The extent of the decay in performance is illustrated by the hexagonal points in Figure 11 which were the second and twelfth tests (Table III) and were run at 10 stoichs makeup air. Although not at identical conditions, corrections for fuel composition and utilization and temperature level should approximately balance. The results indicate a net decay of about 50 mV/cell over the test period.

Post Test Analysis

On December 9, Stack 559 was disassembled at ERC. On the whole, the stack electrochemical components appeared dry while the bipolar plates, on both the anode and cathode sides, had varying degrees of wetness. The wettest plates were at the ends of the stack (Cells 1, 2, 22 and 23). The modifications made to scheme 2 to ensure contact of the acid with the matrices had reduced the area available for acid flow severely in all cells. In addition, the Viton gasket material around Cell 1 (the bottom-most cell) had extruded slightly into the acid fill

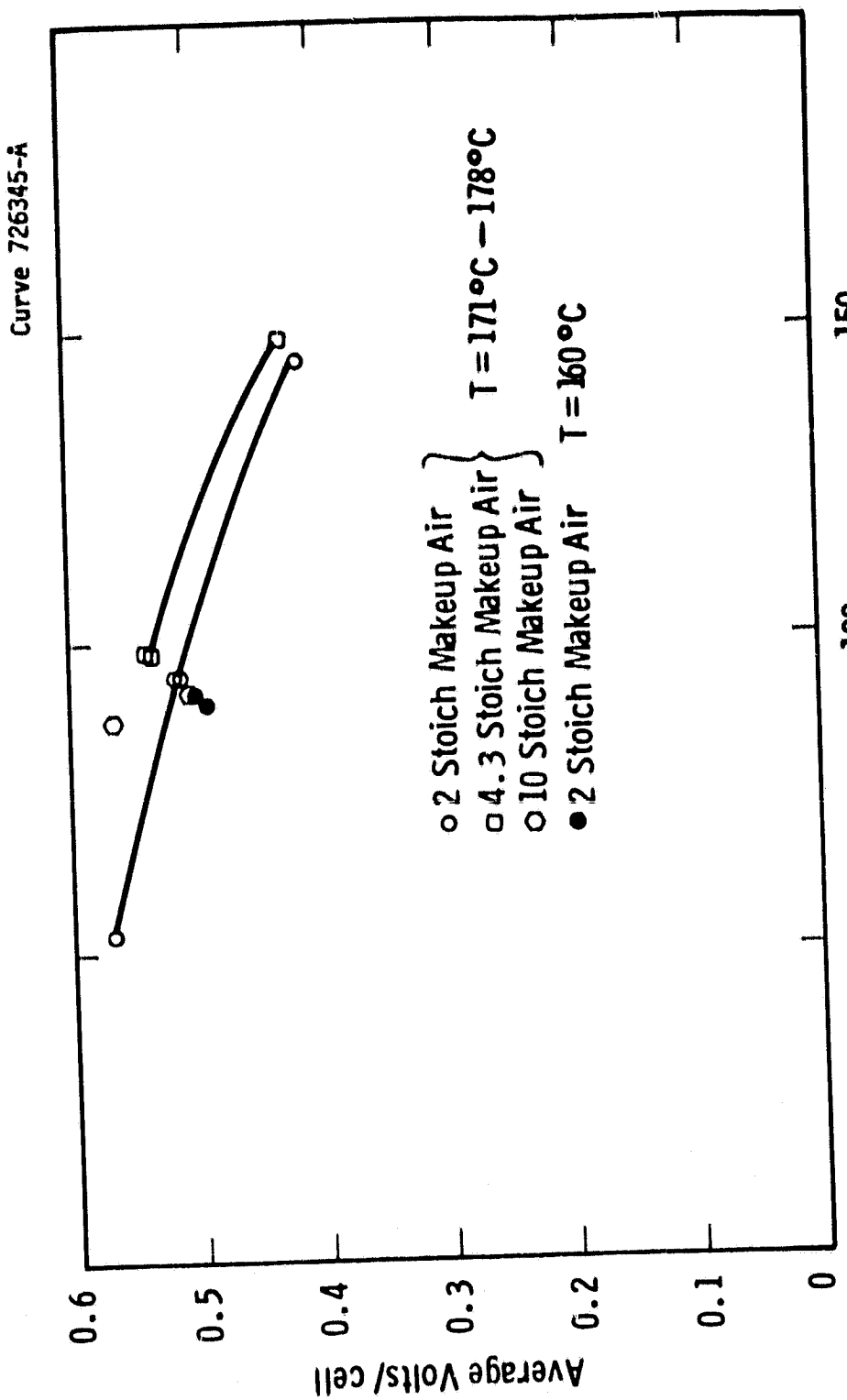

Fig. 11 — Steady state polarization data for Stack 559

tube, partially blocking it. This information will be utilized for future stack fabrication.

When a question concerning the orientation of cooling plates surfaced, the plates were recovered and it was found that the inserted plugs were in the closely spaced channels confirming that hydrogen flow was in the wrong direction.

3.4 Test Stand Construction

During this quarter, a detailed component checkout and several dry runs were made on the 2 kW Test Facility. During this period, pressure transducers were recalibrated, air leaks were sealed, and additional insulation was added to the air loop where needed. The load bank and secondary voltage readout were tested with Stack 559 and found to perform satisfactorily. Also manifold adaptors were designed and fabricated.

Stack 425, built under the DOE Technology Program, was also used to debug the operation of the 2 kW Test Facility. These tests indicated that it was in good working condition and exposed some minor problems (wire connections, grounding, calibration) which were subsequently corrected. The test facility is ready to receive Stack 561.

About 80% of the 8 kW test facility construction work was completed during this quarter. Figure 12 is a schematic diagram of the air loop showing the location of the sensor ports. The anode fuel line, most of the air loop, and the safety system are completed and installation of the 220 VAC line and hood are underway. It is anticipated that the construction work will be completed in February 1981.

All the components for the automatic data acquisition system have been received, and programming work was initiated in late December. A trial run of the program is planned for mid-January and the stack testing program on the 2 kW loop is expected to begin in March.

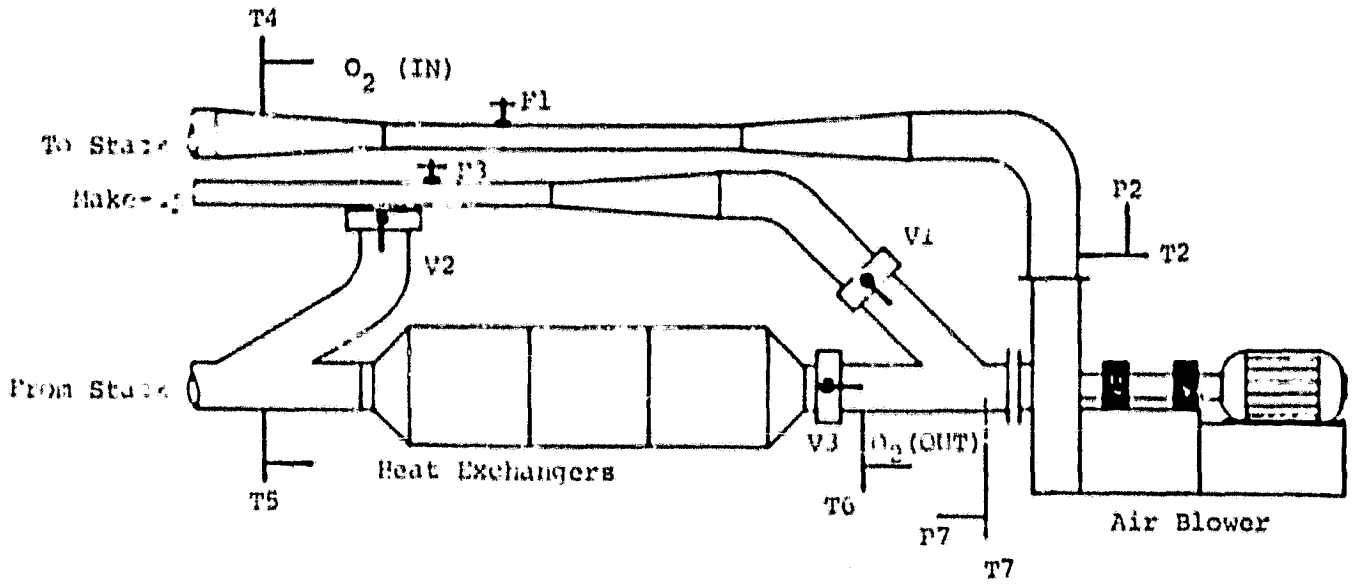

FIGURE 12 THE 8 kW TEST FACILITY AIR LOOP LAYOUT
(with sensor ports shown)

TASK 4: FUEL CONDITIONER DEVELOPMENT

4.1 Fuel and Water Definitions

The required boiler blowdown was established for use in the Operational Requirements Definition of Task 4.2. The following discussion indicates that adequate catalyst and boiler protection can be provided with a blowdown of less than 1 liter/hr.

Boiler blowdown is a function of feedwater solids content and permissible boiler solids content. The specified feedwater solids content (Table VII of the 1st Quarterly Report) is less than 1 ppm by weight for water. Chapter 34, Table 2, of "Steam/Its Generation and Use," Babcock and Wilcox Co., 1972, indicates maximum solids content of 3500 ppm for boilers under 300 psig and recommends that the boiler be operated "well below these limits." From Figure 10 of the B&W reference, a 200 ppm concentration of solids in the boiler was estimated to produce about 50 grams of solids carryover in the steam for 14,000 hours of full load operation. If the reformer catalyst bed removes all of the entrained solids, about 0.2% of the bed void space will be occupied by solids for an average solid density of 1 gram/cc, 50% voids in the catalyst, and a catalyst volume 46 liters. The 200 ppm concentration of solids in the boiler can be maintained with less than 1 liter per hour of boiler blowdown and as much as 2 ppm of solids in the feedwater (equal to resistivity of 0.5 megohm/cm).

4.2 Operational Requirements

Figure 13 is the current version of the Process and Instrumentation Diagram for the fuel conditioning subsystem. The state point data are tabulated for full load and part (1/3) load operation in Tables VI and VII. As explained below, the stream compositions are nearly the same for both conditions and are tabulated in Table VIII.

The operating scenario used for calculating the statepoints and stream compositions assumed a fixed utilization of hydrogen in the

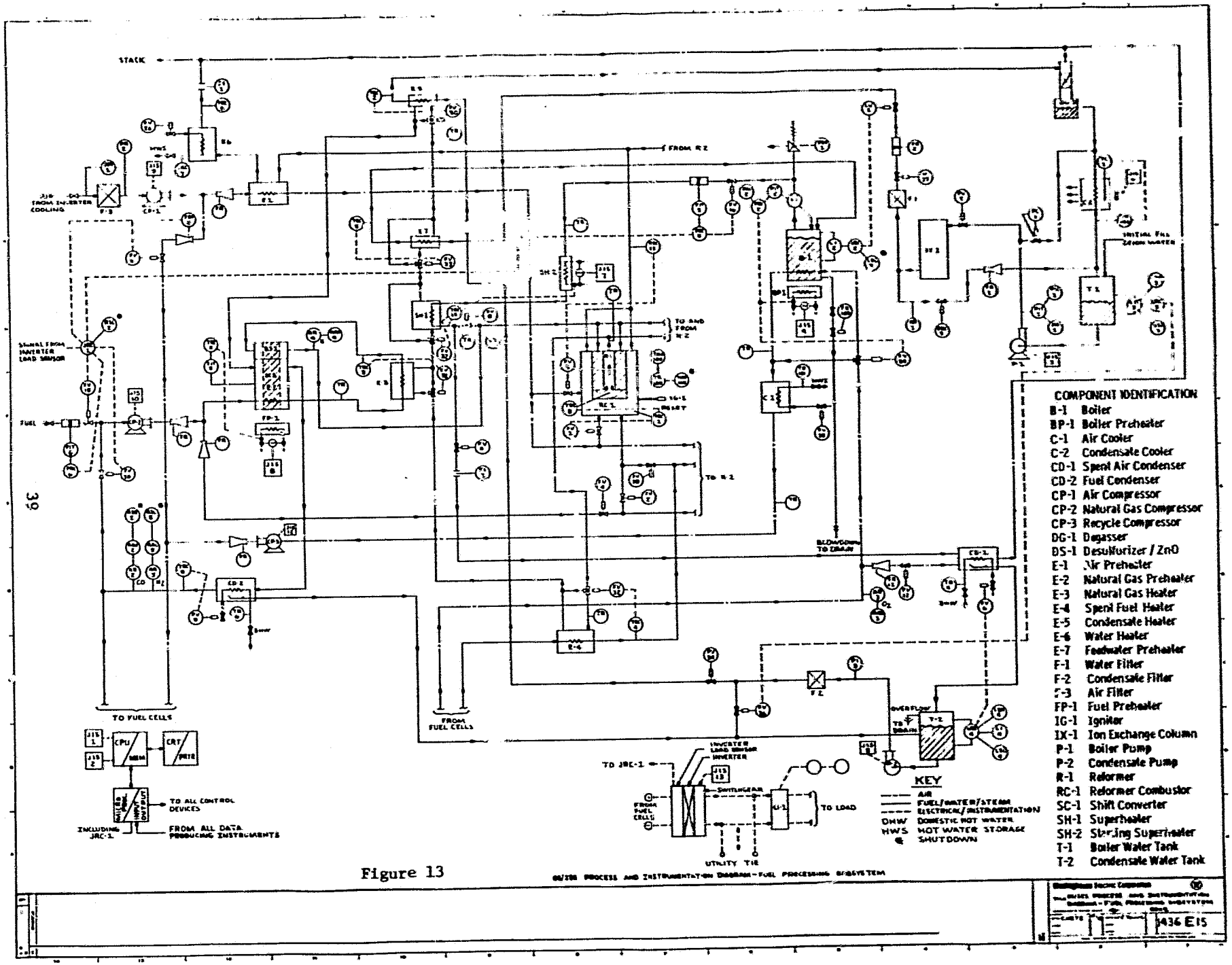
STACK
TO FUEL CELLS
FROM FUEL CELLS
TO JRC-1
FROM FUEL CELLS
TO LOAD
UTILITY TIE
TO ALL CONTROL DEVICES
INCLUDING JRC-1
FROM ALL DATA PRODUCING INSTRUMENTS
BLOWDOWN TO DRAIN
OVERFLOW TO DRAIN
KEY
AIR
FUEL/WATER/STEAM
ELECTRICAL/INSTRUMENTATION
DHW DOMESTIC HOT WATER
HWS HOT WATER STORAGE
SHUTDOWN
COMPONENT IDENTIFICATION
B-1 Boiler
BP-1 Boiler Preheater
C-1 Air Cooler
C-2 Condensate Cooler
CD-1 Spent Air Condenser
CD-2 Fuel Condenser
CP-1 Air Compressor
CP-2 Natural Gas Compressor
CP-3 Recycle Compressor
DG-1 Degasser
DS-1 Desulfurizer / ZnO
E-1 Air Preheater
E-2 Natural Gas Preheater
E-3 Natural Gas Heater
E-4 Spent Fuel Heater
E-5 Condensate Heater
E-6 Water Heater
E-7 Feedwater Preheater
F-1 Water Filter
F-2 Condensate Filter
F-3 Air Filter
FP-1 Fuel Preheater
IG-1 Igniter
IX-1 Ion Exchange Column
P-1 Boiler Pump
P-2 Condensate Pump
R-1 Reformer
RC-1 Reformer Combustor
SC-1 Shift Converter
SH-1 Superheater
SH-2 Starting Superheater
T-1 Boiler Water Tank
T-2 Condensate Water Tank

Figure 13

TABLE VI

STATE POINTS FOR FUEL CONDITIONING SUBSYSTEM AT FULL LOAD (120 kw DC)

	Equipment Item No.	Hot Side (°C) Inlet	Hot Side (°C) Outlet	Cold Side (°C) Inlet	Cold Side (°C) Outlet	Mass Flow (kG/hr) Hot Side	Mass Flow (kG/hr) Cold Side	Thermal Load (kJ/hr)
Air Preheater	E-1	393	230	60	316	290	214	56000
Natural Gas Preheater	E-2	166	248	21	149	103	33	10400
Natural Gas Heater	E-3	328	312	149	204	103	33	4750
Spent Fuel Heater	E-4	388	328	177	316	103	79	17100
Condensate Heater	E-5	232	166	38	100	103	71	18400
Water Heater	E-6	230	121	27	82	290	154	35800
Feedwater Preheat	E-7	282	232	38	85	103	71	14000
Reformer(Both Modules)	R-1	1200	393	204	388	290	103	313000
Spent Air Condenser	CD-1	177	37	10	63	564	1100*	242000
Fuel Condenser	CD-2	248	54	10	63	103	322*	71200
Boiler	B-1	177	158	85	149	7220	71	160000
Superheater	SH-1	312	282	149	204	103	71	8500
Air Cooler	C-1	158	127	27	82	7230	1130	263000
Condensate Cooler	C-2	100	38	21	32	71	1620	18500

* Supplemented by cooling tower water during low domestic hot water demand periods.

TABLE VII

STATE POINTS FOR FUEL CONDITIONING SUBSYSTEM AT ONE-THIRD LOAD (40 kw DC)

Apparatus	Hot Side (°C) Inlet	Hot Side (°C) Outlet	Cold Side (°C) Inlet	Cold Side (°C) Outlet	Mass Flow (kG/hr) Hot Side	Mass Flow (kG/hr) Cold Side	Nominal Thermal Load (kJ/hr)
Air Preheater (E-1)	393	227	60	321	65	48	12890
Natural Gas Preheater (E-2)	183	257	21	181	23	7.3	2910
Natural Gas Heater (E-3)*	328	321	181	204	23**	7.3	440
Spent Fuel Heater (E-4)*	388	328	177	316	23**	18	3850
Condensate Heater (E-5)*	250	183	38	100	23**	16	4150
Water Heater (E-6)	227	121	27	82	65	34	7810
Feedwater Preheater (E-7)*	299	250	38	85	23**	16	3160
Reformer (R-1)(both modules)	1200	393	204	388	65	23	70,480
Spent Air Condenser (CD-1)	177	37	10	63	127	247	54,590
Fuel Condenser (CD-2)	257	54	10	63	23	80	17,740
Boiler (B-1)	177	156	85	149	1605	16	37,980
Superheater (SH-1)*	321	299	149	204	23**	16	1600
Air Cooler (C-1)	157	127	27	82	1620	254	59,480
Condensate Cooler (C-2)	100	38	21	38	16	242	4160

* Utilizes bypass control of hot fluid to provide required cold side outlet temperature.

** Combined mass flow through heat exchanger and bypass valve

TABLE VIII

CHEMICAL COMPOSITIONS OF STREAMS FOR FUEL CONDITIONING SUBSYSTEM IN MOLE FRACTIONS

	Cold Side		Hot Side		Cold Side		Hot Side	
	Inlet	Outlet	Inlet	Outlet	Inlet	Outlet	Inlet	Outlet
	E-1				E-2			
Air	1.0	1.0						
CH_4					0.639	0.639	0.011	0.011
H_2O			0.204	0.204	0.043	0.043	0.257	0.164
H_2					0.234	0.234	0.561	0.554
N_2			0.574	0.574				
O_2			0.081	0.081				
CO					0.023	0.023	0.103	0.009
CO_2			0.141	0.141	0.061	0.061	0.067	0.161
	E-3				E-4			
CH_4	0.639	0.639	0.011	0.011	0.027	0.027	0.011	0.011
H_2O	0.043	0.043	0.257	0.257	0.259	0.259	0.257	0.257
H_2	0.234	0.234	0.561	0.561	0.310	0.310	0.561	0.561
CO	0.023	0.023	0.103	0.103	0.022	0.022	0.103	0.103
CO_2	0.061	0.061	0.067	0.067	0.382	0.382	0.067	0.067
	E-5				E-6			
H_2O	1.0(ℓ)	1.0(ℓ)	0.011	0.011	1.0(ℓ)	1.0(ℓ)	0.204	0.204
H_2			0.257	0.257				
N_2			0.561	0.561			0.574	0.574
O_2							0.081	0.081
CO			0.103	0.103				
CO_2			0.067	0.067			0.141	0.141

TABLE VIII (continuted)

	E-7				R-1&2			
	Cold Side		Hot Side		Cold Side		Hot Side	
	Inlet	Outlet	Inlet	Outlet	Inlet	Outlet	Inlet	Outlet
CH_4			0.011	0.011	0.229	0.011	0.204	0.204
H_2O	1.0(ℓ)	1.0(ℓ)	0.257	0.257	0.656	0.257		
H_2			0.561	0.561	0.084	0.561		
N_2							0.574	0.574
O_2							0.081	0.081
CO			0.103	0.103	0.008	0.103		
CO_2			0.067	0.067	0.022	0.067	0.141	0.141

	CD-1				CD-2			
							0.011	0.012
CH_4								
H_2O	1.0 (ℓ)	1.0 (ℓ)	0.25	0.109	1.0(ℓ)	1.0(ℓ)	0.164	0.115
H_2							0.654	0.692
N_2			0.69	0.819				
O_2			0.06	0.072				
CO							0.009	0.009
CO_2							0.161	0.171

TABLE VIII (continued)

	Cold Side		Hot Side	
	Inlet	Outlet	Inlet	Outlet
		B-1		
CH_4				
H_2O	1.0 (ℓ)	1.0 (g)	0.25	0.25
H_2				
N_2			0.69	0.69
O_2			0.06	0.06
CO				
CO_2				
		C-1		
Air				
H_2O	1.0(ℓ)	1.0(ℓ)	0.25	0.25
N_2			0.69	0.69
O_2			0.06	0.06

	Cold Side		Hot Side	
	Inlet	Outlet	Inlet	Outlet
		SH-1		
			0.011	0.011
1.0 (g)	1.0(g)		0.257	0.257
			0.561	0.561
			0.103	0.103
			0.067	0.067
		C-2		
1.0	1.0			
			1.0(ℓ)	1.0(ℓ)

fuel cells and a fixed composition of spent fuel. This implies that the reformer temperature will be reduced at part load to hold methane conversion efficiency down which should contribute to more reliable, longer lived reformer operation. This also permits the reformer heat requirements to be met by spent fuel so no supplementary methane is required for steady part load operation. This scenario is a reasonable one and we will continue to use it in our definition of operational requirements until adequate information is developed on overall system operation to define a more appropriate scenario.

4.3 Catalyst Data Base

4.3.1 Shift Converter Catalyst Test

Carbon monoxide shift experiments using United Catalyst C-18HC in crushed (0.5 mm) and pelleted (2.34 x 2.39 mm) forms and Catalyst 201 in crushed (0.5 mm) and pelleted (2.39 x 2.39 mm) forms were completed this quarter.

The catalysts are shipped in the oxidized form and were reduced before testing following the manufacturer's recommendations This involved carefully controlling the hydrogen concentration to maintain the temperature of the catalyst bed under 260°C for a period of 8 hours and maintaining the space velocity of the reducing gas (inert gas and hydrogen) between 200 and 1500 hr^{-1}.

Figures 14 and 15 show the results for UC C-18HC and Catalyst 201, respectively. A comparison of the data is shown in Table IX. The results can be summarized as follows:

1. The rate of reaction for UC C-18HC is first order in CO and is independent of H_2O concentration. However, the rate of reaction for Catalyst 201 is first order in both CO and H_2O. This dissimilarity may be due to difference in the catalyst supports which are zinc and aluminum oxides for UC C-18HC and zinc and chromium oxides for Catalyst 201.

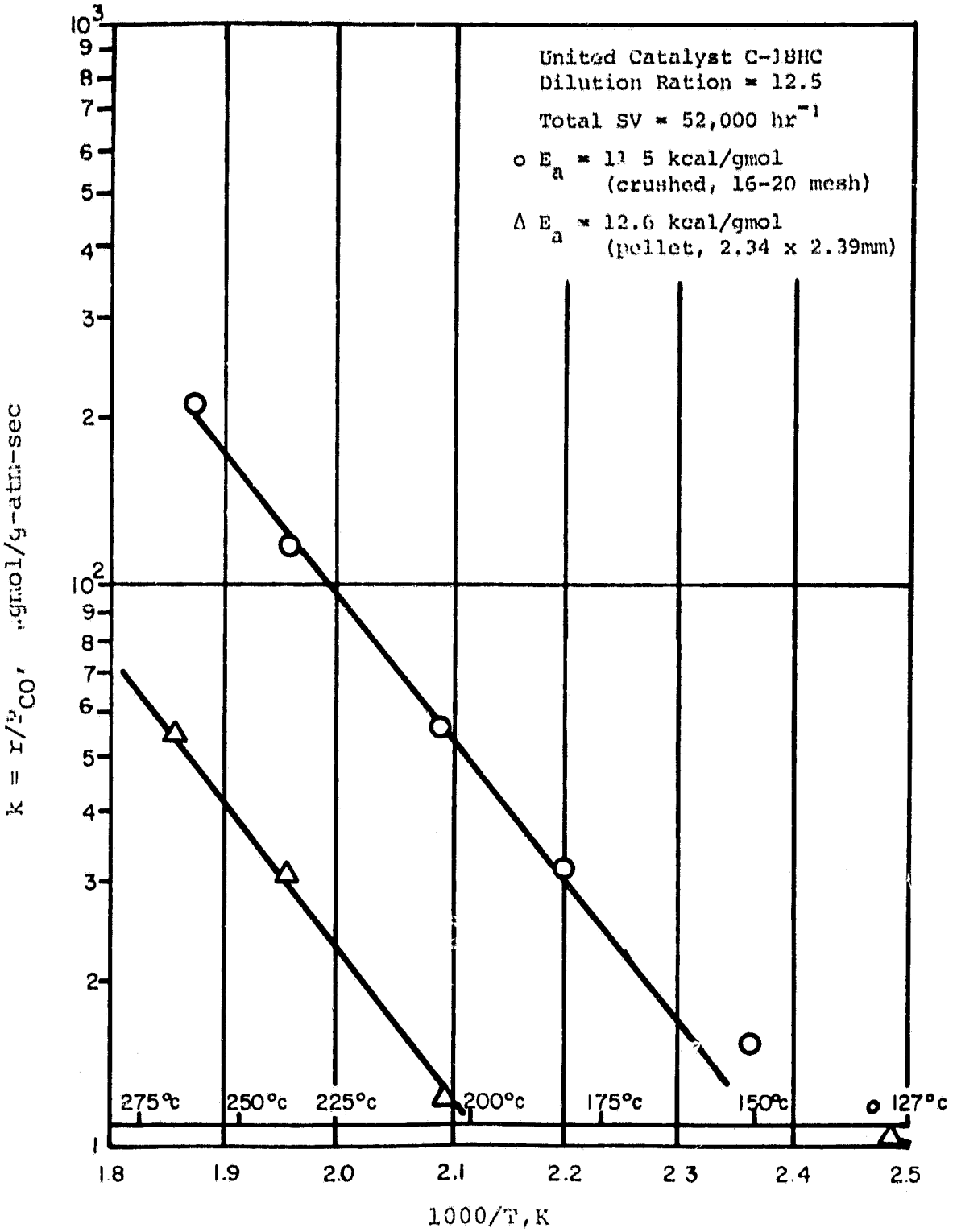

FIGURE 14. ARRHENIUS PLOT FOR SHIFT CATALYST UC C-18HC, CRUSHED

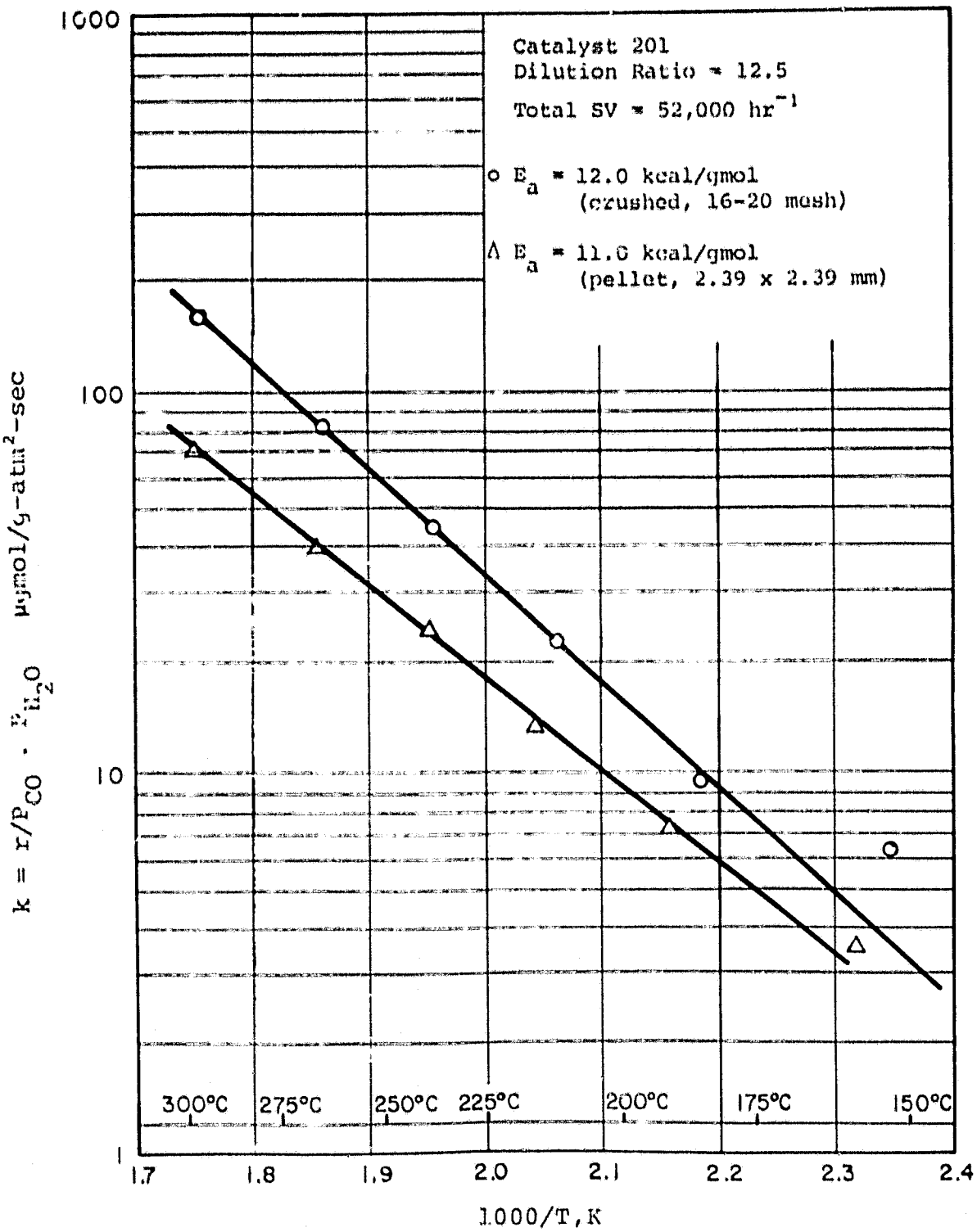

FIGURE 15. ARRHENIUS PLOT FOR SHIFT CATALYST 201

TABLE IX

COMPARISON OF CO SHIFT CONVERTER CATALYSTS

CATALYST‡	TYPE	ACTIVATION ENERGY, kcal/gmol	AT 204°C (400°F)	
			ΔT_{radial},* °C	ACTIVITY μgmol/g-atm-sec
UC C-18HC	Crushed	11.5	-2	55
UC C-18HC	Pelleted	12.6	-1	13
201	Crushed	12.0	-2	48†
201	Pelleted	11.0	-2	28†

* $\Delta T_{radial} = T_{wall} - T_{bed}$, °C

† Catalyst activity measured at $P_{H_2O} = 0.26$ atm

‡ UC C-18HC: $r = k \cdot P_{CO}$

Catalyst 201: $r = k \cdot P_{CO} \cdot P_{H_2O}$

2. The catalysts have activation energies, from 11.0 to 12.0 kcal/gmol.

3. The activity of Catalyst 201 depends on the water partial pressure but, at P_{H_2O} = 0.26 atm., UC C-18HC has only a slightly higher activity than Catalyst 201 (55 vs 48 μgmol/g-atm-sec at 204°C).

4. For UC C-18HC, the crushed catalyst has much higher activity than the pelleted catalyst (55 vs 13 μgmol/g-atm-sec at 204°C). When the experiments were repeated, the same results were obtained. Since the activation energy is similar for both crushed and pelleted catalysts, it is assumed that diffusion will have little effect on the catalyst activity. The pelleted activity, to be used for design, must be lower due to loss of available active catalyst sites due to the pellet forming process.

5. For Catalyst 201, the crushed catalyst has slightly higher activity than the pelleted catalyst (48 vs 28 μgmol/g-atm-sec at 204°C) but a similar activation energy (12.0 vs 11.0 kcal/gmol). There is no evidence to indicate a diffusion effect in the testing temperature range (150°C to 275°C).

The choice of which catalyst to use in the shift reactor design will be made on the basis of the most active catalyst for the actual gas composition (H_2O partial pressure) used for design.

4.3.2 Reforming Aging Test

The methane reforming aging test was initiated in October and completed in December with a total test time of 1630 hours. A total mass of 22.7 g (volume = 19.3 cc) of catalyst 100 was used in pellet form (1.25 x 1.25 mm). The experimental results are shown in Figure 16.

Table X compares the fresh catalyst conversion and that calculated for equilibrium conditions at 585°C and a SV of 1500 hr^{-1}. At 1500 hr^{-1}, the methane conversion decreased from a fresh catalyst conversion of 69% to a steady value of 64% in a period of 35 hours.

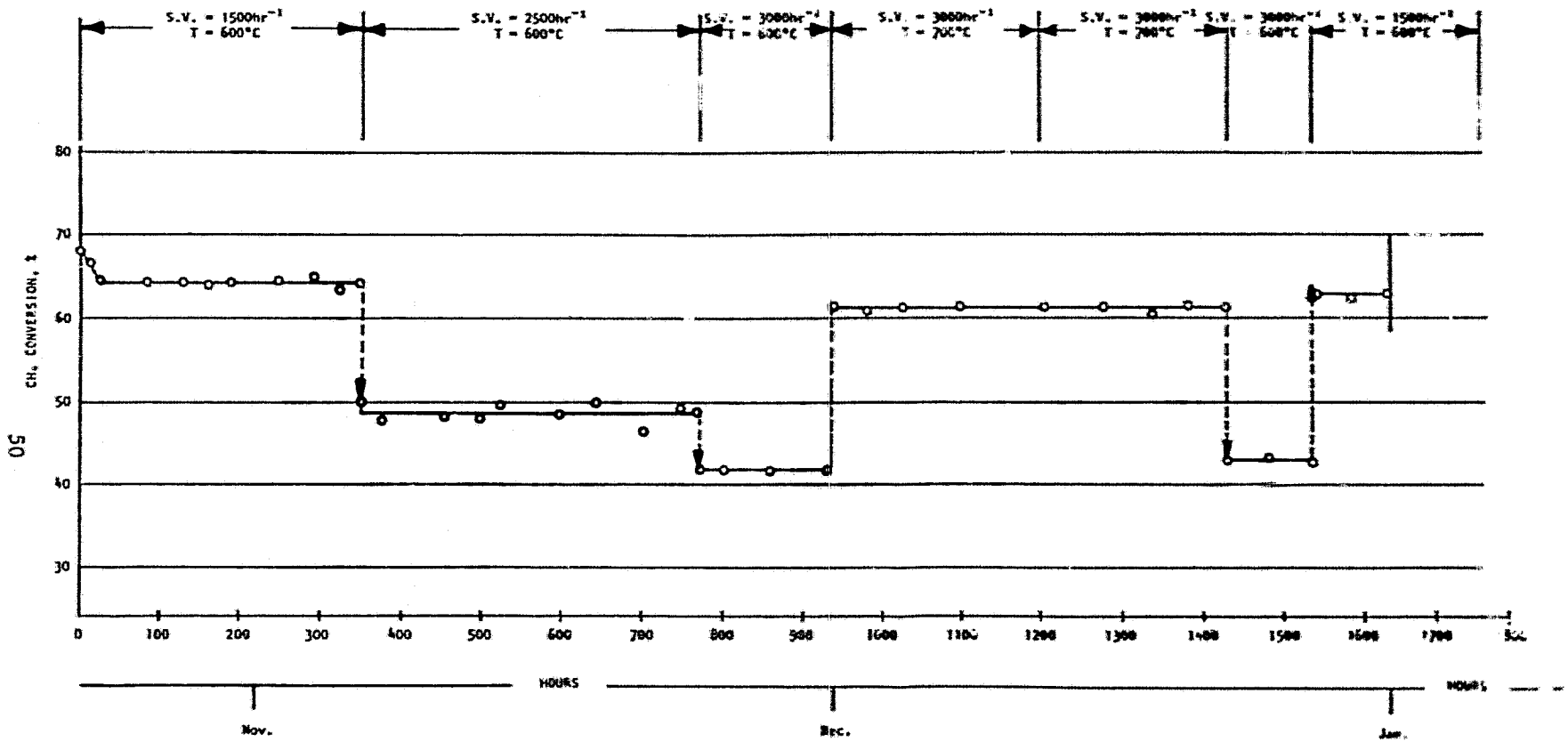

Figure 16. METHANE REFORMING AGING TEST

TABLE X

STEAM REFORMING AGING TEST

(Fresh Catalyst)

Catalyst - Catalyst 100

Catalyst Weight - 22.7g (catalyst volume = 19.3 cc)

CH_4 Space Velocity - 1500 hr^{-1}

Inlet Feed:

CH_4 - 28.962 ℓ/hr

H_2O - 86.886 ℓ/hr

H_2 - 2.896 ℓ/hr

Reactor Temperature, °C:

	Wall	Bed
Exit (in Catalyst)	611	559
Middle of Bed	619	549
Inlet(Prior to Catalyst)	635	604

Results:

		Test	Equilibrium (585°C)
CH_4 Conversion,%:		67.6	70
Dry Gas,%:	CH_4	0.118	0.082
	H_2	0.635	0.727
	CO	0.073	0.067
	CO_2	0.174	0.124

Extending the operating time to 350 hours showed no further decay. Since the methane conversion of 64% is close to the equilibrium conversion (70%) at 600°C (and such operation reduces the sensitivity of aging tests), the space velocity was increased to 2500 hr^{-1}. At 2500 hr^{-1}, the methane conversion was constant at a value of 49% for 440 hours.

In preparation for increasing the temperature to 700°C, the space velocity was increased to 3000 hr^{-1}. No decay occurred during the subsequent 140 hrs of operation at 600°C and the temperature was increased to 700°C. The methane conversion was constant at 62% for a period of 490 hours. When the temperature was decreased to 600°C, the methane conversion was the same as (or slightly better than) before for this condition.

After the initial break-in period, catalyst 100 suffered no decrease in activity during 1630 hours of testing on research-grade methane. Operation at a temperature as high as 700°C caused no deactivation of the catalyst, indicating that sintering and loss of surface area did not occur.

4.4 Ancillary Subsystem Data Base

Burner Development

The burner test rig was commissioned and initial tests on natural gas (specified start-up fuel) and simulated spent fuel were made. These tests included preheat of the fuel and air to the design temperature but no humidification of the fuel gas stream since the vaporizer was not installed. On spent fuel the flame was excessively long and CO content was high indicating poor mixing of the fuel and air streams and inefficient combustion. The burner was modified and reinstalled in this rig and tests will continue in the next quarter.

Heat Exchangers

During this quarter, heat exchanger performance specifications were prepared for 12 heat exchangers used in the fuel conditioner subsystem. These specifications were based on heat balance calculations performed on the hot and cold sides of the exchangers. Steady state requirements for both full power and one-third power operation were included, and were based on data from Tables VI to VIII in Section 4.2 of this report.

As an example, Table XI is the specification for the air preheater Item E-1 of the P&I diagram (Figure 13). These specifications are being sent to the exchanger vendors who responded affirmatively to the inquiry sent out during Phase I of this program. Complete sets of the exchanger specifications are being sent to the NASA Project Monitor and JPL for review and comment.

Controls and Instrumentation

The control functions required to start, change load and hold a steady load were worked out and an automatic starting sequence had been worked out and the needed instrumentation and controls were defined for the fuel processing subsystem. These are shown on the P&I diagram (Figure 13).

The system control will be programmed to follow the electrical load during a transient condition. To control the hot water portion, it may be necessary to cool the water via a cooling tower. It may also be necessary to waste heat by bypassing some of the heat exchangers of the fuel conditioning subsystem. Overrides will be provided to protect the system in the case of conditions such as low water level, over temperature, and low fuel quality.

Steam Ejector

Penberthy has assured that the idea of using a steam ejector to replace the natural gas compressor is feasible. They have tests

STEADY STATE HEAT TRANSFER REQUIREMENTS

FULL POWER NORMAL DUTY SPECIFICATION

NAME/NUMBER: Air Preheater/E-1

SERVICE: Gas to Air[1]

Maximum Heat Duty, kJ/Hr, (BTU/Hr): 56,150 (53,180)

	Hot Side		Cold Side	
Mass Flow Rate, kg/Hr, (lb/Hr)	290(639.3)		214(471.8)	
	Inlet	Outlet	Inlet	Outlet
Composition, mol fraction				
CH_4				
H_2O	0.204	0.204		
H_2				
N_2	0.574	0.574	Air	Air
O_2	0.081	0.081		
CO				
CO_2	0.141	0.141		
Molecular Wt	28.552		28.970	
Fluid Properties				
Density, kg/m^3, (lb/ft^3)				
Therm. Cond., W/m^2 °C, (BTU/Hr ft^2 °F)				
Sp. Heat, kJ/kg°C, (BTU/lb°F)	1.1849(0.2830)		1.0241(0.2446)	
Viscosity, Pa·S, (lb/ft hr)				
Temperature, °C, (°F)	393(739.4)	230(446)	60(140)	316(600.8)
Pressure, kPa, (psia)	106.1(15.39)	103.8(15.06)	17.6(17.05)	115.3(16.72)
ΔP, kPa, (in H_2O)	2.24(9)		2.24(9)	

Notes: (1) Sulfur free products of combustion/Compressed, filtered air.

Table XI - Sample of Heat Exchanger Specification

STEADY STATE HEAT TRANSFER REQUIREMENTS

ONE-THIRD POWER NORMAL DUTY SPECIFICATION

NAME/NUMBER: Air Preheater/E-1

SERVICE: Gas to Air

Heat Duty, kJ/Hr, (BTU/Hr): 12,850(12,170)

	Hot Side		Cold Side	
Mass Flow Rate, kg/Hr, (lb/Hr)	65(143.3)		48(105.8)	
	Inlet	Outlet	Inlet	Outlet
Composition, mol fraction				
CH_4				
H_2O	0.204	0.204		
H_2				
N_2	0.574	0.574	Air	Air
O_2	0.081	0.081		
CO				
CO_2				
Molecular Wt	28.552		28.970	
Fluid Properties				
Density, kg/m^3, (lb/ft^3)				
Therm. Cond., W/m^2 °C, (BTU/Hr ft^2 °F)				
Sp. Heat, kJ/kg°C, (BTU/lb°F)	1.1844(0.2829)		1.0245(0.2447)	
Viscosity, Pa·S, (lb/ft hr)				
Temperature, °C, (°F)	393(739.4)	227(440.6)	60(140.0)	321(609.8)
Pressure, kPa, (psia)				
ΔP, kPa, (in H_2O)				

Table XI (continued)

and analyses in progress and we should receive the report during the next quarter.

4.6 10 kW Reformer Design

Table XII presents the design data for a 10 kW reformer and shift converter. The data are based on the 502.2 gmol/hr hydrogen required for a 10 kW fuel cell at 65% utilization. The catalysts needed for the reformer and the shift converter are 2.29ℓ (0.0808 ft^3) and 14.10ℓ (0.5 ft^3) respectively.

4.7 Prototype Conceptual Design

The reformer and shift converter designs will be started in January. The reformer design and manufacturing cost estimate will be based on the concept embodied in Westinghouse Disclosure No. AL80-22. The shift converter design will be similar to UTC's 40 kW unit converter/HDS/ZnO package system.

TABLE XII

DESIGN DATA FOR 10 kW REFORMER AND SHIFT CONVERTER*

COMPONENT	IN		OUT	
	kg/hr	MOLE FRACTION	kg/hr	MOLE FRACTION
	REFORMER			
CH_4	1.9708	0.229	0.1312	0.011
H_2O	6.3464	0.656	3.5609	0.257
H_2	0.0904	0.084	0.8633	0.561
CO	0.1175	0.008	2.2198	0.103
CO_2	0.5243	0.022	2.2742	0.067
TOTAL:	9.0494	0.999	9.0494	0.999
Total catalyst volume = 2.29ℓ CH_4 space velocity = 1200 hr^{-1} Steam/carbon mole ratio = 2.865				
	SHIFT CONVERTER			
CH_4	0.1312	0.011	0.1353	0.011
H_2O	3.5609	0.257	2.2696	0.164
H_2	0.8633	0.561	1.0049	0.654
CO	2.2198	0.103	0.1937	0.009
CO_2	2.2742	0.067	5.4459	0.161
TOTAL:	9.0494	0.999	9.0494	0.999
Total catalyst volume = 14.1ℓ CO space velocity = 125 hr^{-1} Steam/carbon mole ratio = 1.51				

* H_2 required for 10 kW fuel cell = 502.2 mol/hr (65% utilization)

TASK 5: MANAGEMENT REPORTING AND DOCUMENTATION

5.1 Supervision and Coordination

A combined progress review and fuel cell stack design review meeting was held on November 5 and 6 at the Westinghouse R&D Center. As a result of open discussions during this meeting, several decisions were made and implemented:

1. All future stacks for this program will use "heat-treated" bipolar and cooling/bipolar plates. This included the cooling/bipolar plates for Stack 561 which were already assembled. As discussed under "Short Stack Fabrication," these were successfully heat treated and included in the stack.

2. The NASA Project Manager requested that the documentation of the stack fabrication and procedures be revised to reflect recent changes. A draft of a revised document was prepared and submitted for his review.

3. Vareum resin will be used in all future moldings of bipolar, end and bipolar/cooling plates for this project. The existing plates, which contain Colloid resin, will be used for Stacks 560, 561 and 562. Blanks for bipolar, cooling/bipolar, and end plates for Stack 563 were molded with Vareum.

4. An explanation of the rationale for the strategy of temperature changes adopted for the reforming catalyst aging tests was submitted to the NASA Project Manager as he requested in the meeting.

5. The NASA Project Manager requested that the Westinghouse and ERC fuel conditioner task leaders select a configuration for the 10 kW reformer and submit a description of it and an explanation of the selection for his approval. As described under the Fuel Conditioning Task, a design was selected and the description will soon be submitted for approval.

A number of informal meetings and discussions were held among potential contributors to future work and the personnel developing the formal plan for future work. The scope of the technical efforts required to meet the overall objectives of the program were determined and formed the basis for task descriptions and estimates of effort for the plan.

5.2 Documentation and Reporting

Patent approvals for the Technical Status Reports for July and August were received and they were distributed in accordance with the NASA supplied lists. The Fourth Quarterly Report and the Technical Status Reports for October and November were submitted for NASA patent approval. The management reports (533M and 533P) for October and November were prepared and submitted along with additional cost and manhour graphs. The financial plan for the Sixth Quarter (533Q) was prepared and submitted.

5.3 Planning

A plan for the program (from a conceptul system design through field testing of three (3) OS/IES systems) was developed. The plan covers the period from October 1981 to mid 1986. The plan includes a Work Breakdown Structure (WBS), task descriptions, and estimates of manpower and costs in compliance with the WBS and Program Schedule. This plan was submitted to the NASA Project Manager.

III. PROBLEMS

The assembly of Stacks 560 and 561 is halted pending submission of documents describing the revised fabrication procedures to NASA Project Manager and his approval of them. The revised procedures reflect the decisions to use heat treated plates and the original acid fill Scheme 2 and other details associated with them. These changes should increase the probability of success and improve the stack performance but will result in increased costs (per stack) and probably require time extensions.

IV. PLANS

TASK 1: DESIGN OF LARGE CELL STACKS

Based on the temperature data obtained from Stack 561, the cooling plate design for Stack 563 will be finalized.

The document describing Stacks 560, 561, 562 and 563 will be revised as needed and submitted to the NASA Project Manager.

The data on shrinkage during heat treatment will be reviewed and a decision to cement cooling plate halves prior or subsequent to heat treatment will be made.

The analysis of the distribution of the stack compression forces between the active cell area and the boundary or shim area using the recently acquired material data is continuing. Available data on the effects of stack compression or performance will be reviewed and correlated with the model.

A plan for evaluating several approaches to modular assembly of stacks will be developed and implemented.

TASK 2: STACK FABRICATION

All subassemblies for Stacks 560 and 561 are complete and assembly will take place early in the next quarter.

Heat-treatment of the bipolar and cooling plates for Stack 562 will be scheduled once the remainder of the plates are received from machining. This is expected to take place in mid-January. Cell subassemblies and final stack assembly are scheduled for completion by mid-February.

The bipolar/cooling plates for Stack 563 will be machined. Heat-treatment will be scheduled as soon as the plates are received from the vendor. This will be followed by cell subassembly and stack assembly, scheduled for completion by the end of February.

TASK 3: STACK TESTING

Pretesting and testing of Stacks 561 and 560 will be initiated as soon as fabrication is complete. This should occur early in the first month of the next quarter.

Immediately following pretesting Stack 561 will be installed and tested in the OS/IES simulation loop. The primary purpose of these tests will be to obtain temperature profile data with the innovative cooling plates under OS/IES operating conditions. This information will verify and be used in fine tuning of the detailed analytical model and will provide the design basis for the cooling plates of Stack 563.

Test runs of the 8 kW test facility have shown that it is in good working condition and it will be used for testing Stack 561 and future 2 kW stacks.

Work will continue on the sealing and insulation of the air loop, and on the installation of the anode gas preheater for the 8 kW test facility.

Dry runs will be conducted to detect any problem associated with the operation of the loop's flow components. Work will be initiated on the electrical wiring in the early part of next quarter.

Programming of the Data Acquisition System (which is shared between the 2 kW and the 8 kW test facilities) is expected to be completed by mid-March.

The testing of Stack 561 in the OS/IES loop will be extended to 24 hr/day operation as experience with the automatic control features is gained. The 2 kW test facility is also designed for unattended operation and will be used for 24 hr/day tests when needed.

Construction of the 8 kW test facility will continue.

TASK 4: FUEL CONDITIONER DEVELOPMENT

The analysis of the system performance and control requirements will continue.

The design of the reformer and shift converter test rig will continue and construction should be nearly completed during the next quarter.

The computer model will be extended to be applicable to the double counterflow configuration required by our present reformer concept. A letter is being prepared for submittal to appropriate reformer design and catalyst sales organizations to solicit their help in the double counterflow model adaptation and in future system design and/or fabrication efforts. This letter, based on comments received from JPL, will be mailed to interested parties in early January.

Installation of the burner rig water vapor generator will be completed early next month and the revised burner will be tested for combustion efficiency and to establish its operating envelope. Further modifications will be made as needed.

TASK 5: MANAGEMENT AND DOCUMENTATION

Coordination of efforts among the task leaders and between ERC and Westinghouse will be continued.

Technical review meetings will be held at the convenience of the NASA Project Manager and presentations to and meetings with DOE personnel will be scheduled as requested.

A meeting to coordinate the parallel ERC technology program is planned for the next quarter. Several key members of the OS/IES project team will attend.

The task leaders' inputs to the Technical Status Reports will be edited and the reports will be submitted to the NASA Project Manager for patent approval. The management reports will also be prepared and submitted to the NASA Project Manager.

This report, the 4th Quarterly and the October and November technical narratives, will be distributed when approved by the NASA Project Manager.

As described in Section II, a plan prepared by the Westinghouse Advanced Energy Systems Division was submitted to the NASA Project Manager and a meeting to review it is planned for the next quarter.